Exolith Martian Simulants Constituent Report

exolithlab@ucf.edu

July 2023

Table of Contents

1 Context

Our goal is to develop and produce high-fidelity mineralogical simulants for the Moon, Mars, and asteroids. While one could make a chemically similar simulant for well-characterized planetary regolith using laboratory grade oxides, such a simulant would poorly reproduce many important regolith properties, including geotechnical properties. Mineralogy is the primary driver of these properties so we aim to simulate mineralogy in the correct proportions. Inevitably, naturally-occurring terrestrial minerals have experienced weathering and will contain at least small amounts of undesired mineral phases (contaminants). To control the quality of Exolith feedstock and identify reliable mineral sources with minimal contaminant phases, we verify the composition of each simulant constituent regularly.

The combination of X-ray fluorescence (XRF) and X-ray diffraction (XRD) techniques constrains mineral composition and can be used to identify the presence of contaminant phases. XRF analysis reveals the chemical composition of a sample. XRD analysis reveals crystal lattice spacing characteristic of particular mineral phases. The XRF and XRD data were acquired at the University of Central Florida's Materials Characterization Facility (MCF), with an exception for the basalt data as described in that section. All samples studied at the MCF were prepared as powders. The XRF data were acquired with a PANalytical Epsilon 1 XRF and concentrations of each compound were determined using Omnian software. The Epsilon 1 XRF uses a 50-kV silver X-ray tube. XRD data were acquired using a PANalytical Empyrean XRD Diffractometer. The Empyrean uses a 1.8-kW copper X-ray tube and a vertical goniometer with theta, theta geometry. We used HighScore software connected to the International Centre for Diffraction Data Powder Diffraction File to aid in XRD interpretation.

In 2021, reflectance spectra were obtained by Takahiro Hiroi at the Keck/NASA Reflectance Experiment Laboratory (RELAB; **http://www.planetary.brown.edu/relab/**). Visible-to-near-infrared spectra were obtained using a UV-Vis-NIR bidirectional reflectance spectrometer with an incidence angle of 30◦ and emergence angle of 0◦. Mid-infrared (thermal) spectra were obtained using a Thermo Nexus 870 FT-IR spectrometer.

Particle size analysis was conducted through a combination of sieve analysis and laser diffraction size analysis. Using a Gilson SS-14 Orbital Sieve Shaker, constituent minerals were analyzed down to 500 microns. A CILAS 1190 Laser Particle Size Analyzer was utilized at sizes less than 500 microns, and the two graphs (sieve and laser) were combined.

There have been 3 different batches of simulant constituents since the founding of the Exolith Lab, defined by the basalt source used:

Pebble Junction Basalt (Before 06/01/2021)

Butler Basalt (06/01/2021-07/31/2023)

Merriam Crater Basalt (08/01/2023-Present)

Batch numbers are provided on each simulant's website page, providing the appropriate spec sheet for each batch.

2 Simulant Constituent Analysis

2.1 Anorthosite

- Description: Igneous rock rich in plagioclase feldspar
- Source: Hudson Resources, Inc. GreenSpar
- Idealized Formula: $CaAl_2Si_2O_8$ (anorthite); $NaAl_2Si_2O_8$ (albite)

Notes Major phase anorthite confirmed by XRD analysis (Figure 2, Table 1). Presence of small quantities of albite also confirmed by XRD. The Hudson Resources website[1] reports that the GreenSpar Anorthosite product is 90% plagioclase feldspar. Our XRF findings (Table 2) are consistent with those reported by Hudson and with the XRD results.

Figure 1. Photo of Anorthosite

2.1.1 X-Ray Diffraction Pattern

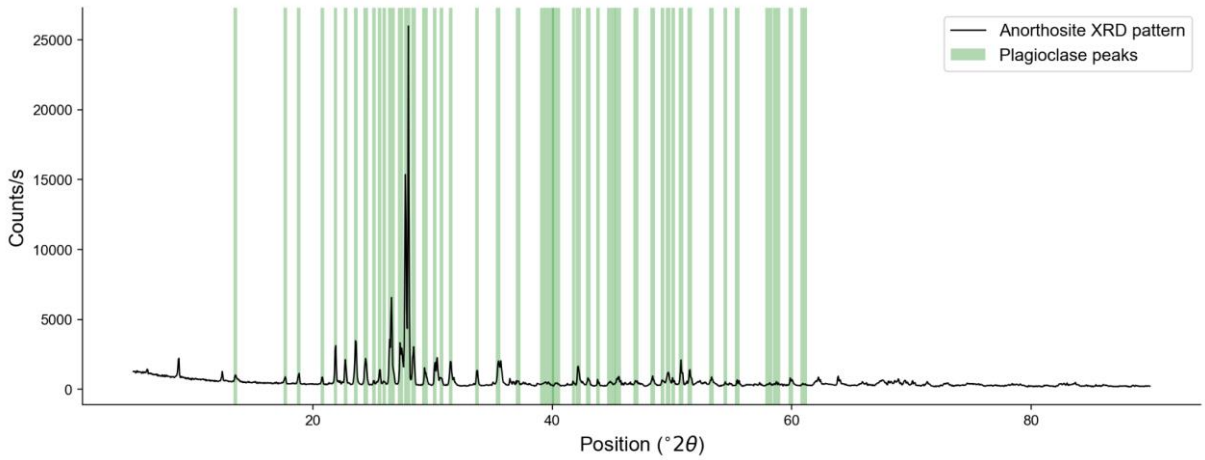

Figure 2. XRD pattern for Anorthosite sample. [1]https://hudsonresourcesinc.com/

Table 1. Anorthosite - XRD Pattern Peaks

Position (°2θ)	*Relative Intensity (%)*	*d-spacing (Å)*	*Matched By*
5.89	5.3	15.00	
8.80	10.0	10.05	
12.44	4.9	7.11	
13.55	4.1	6.53	Anorthite, albite
17.70	3.2	5.01	Anorthite
18.83	4.3	4.71	Anorthite, albite
20.79	3.5	4.27	Anorthite
21.90	15.1	4.06	Anorthite, albite
22.73	9.7	3.91	Anorthite, albite
23.59	17.6	3.77	Anorthite, albite
24.42	10.2	3.65	Anorthite, albite
25.10	2.2	3.55	Anorthite
25.60	6.2	3.48	Anorthite, albite
25.96	1.7	3.43	Anorthite, albite
26.57	31.9	3.35	Anorthite, albite
27.33	14.5	3.26	Anorthite
27.73	73.3	3.22	Anorthite, albite
28.01	100.0	3.19	Anorthite, albite
28.42	14.0	3.14	Anorthite, albite
29.37	5.6	3.04	Anorthite
30.19	8.2	2.96	Anorthite, albite
30.74	3.0	2.91	Anorthite, albite
31.51	9.1	2.84	Anorthite, albite
33.73	5.8	2.66	Anorthite, albite
35.49	8.9	2.53	Anorthite, albite
37.16	1.9	2.42	Anorthite, albite
39.56	1.2	2.28	Albite
40.31	1.1	2.24	Albite
41.78	1.5	2.16	Albite
42.17	7.4	2.14	Albite
43.02	2.7	2.10	Albite
43.83	1.9	2.07	Albite
44.90	1.5	2.02	Albite
45.49	2.8	1.99	Albite
46.99	1.9	1.93	Albite
48.39	3.5	1.88	Albite
49.19	2.3	1.85	Albite
49.68	5.1	1.84	Albite
50.11	1.9	1.82	Albite
50.76	7.8	1.80	Albite
51.49	6.0	1.77	Albite
53.31	3.1	1.72	Albite
54.45	1.4	1.69	Albite
55.46	2.1	1.66	Albite
58.08	0.9	1.59	Albite
58.72	1.2	1.57	Albite
59.91	2.6	1.54	Albite
60.99	0.8	1.52	Albite
62.22	3.4	1.49	
63.86	3.7	1.46	
65.83	1.2	1.42	
67.62	2.2	1.39	
68.89	2.5	1.36	
69.42	2.1	1.35	
70.06	1.9	1.34	
71.30	1.6	1.32	
72.91	1.1	1.30	
74.87	1.0	1.27	
78.44	0.7	1.22	
82.37	0.8	1.17	
83.65	1.1	1.16	
85.96	0.3	1.13	

Peak match citation: PDF 98-002-2022 (anorthite), PDF 98-000-9830 (albite) in Gates-Rector and Blanton (2019)

2.1.2 Chemistry from X-Ray Fluorescence

Table 2. Anorthosite - Bulk Chemistry

Compound	*Concentration (wt%)*
Al_2O_3	29.4
SiO_2	49.3
P_2O_5	1.0
SO_3	0.1
Cl	0.1
K_2O	0.3
CaO	19.0
TiO_2	0.1
Fe_2O_3	0.7
Total	100.0

2.1.3 FTIR Spectroscopy

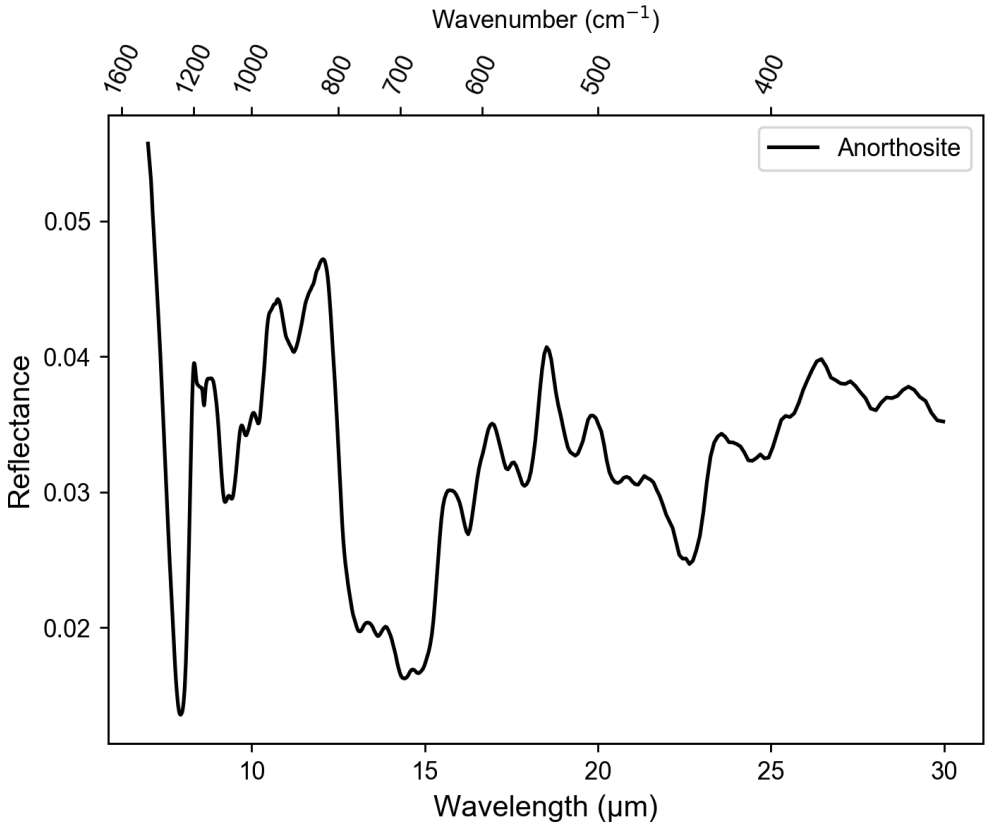

Figure 3. Anorthosite FTIR Spectroscopy

2.1.4 VIS NIR Spectroscopy

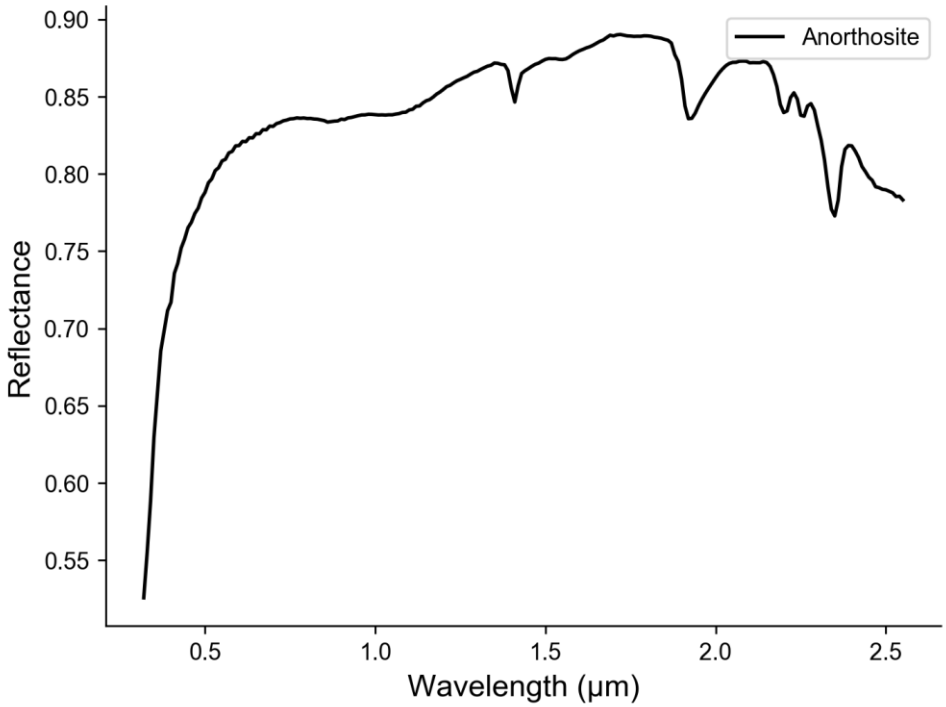

Figure 4. Anorthosite VIS NIR Spectroscopy

2.1.5 Particle Size Analysis

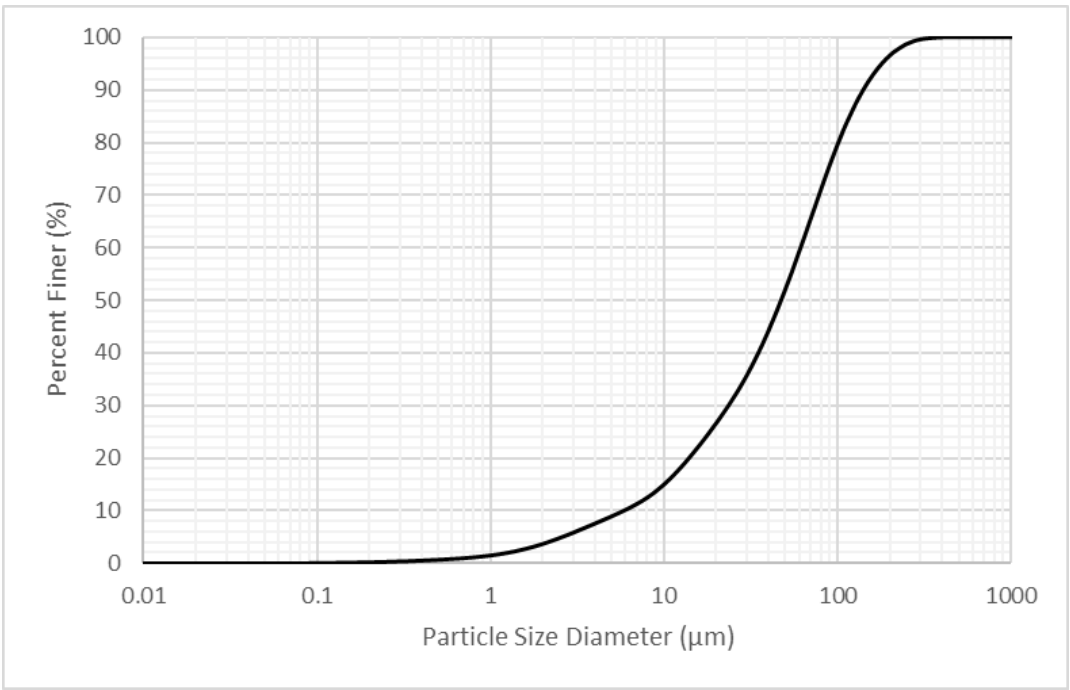

Figure 5. Anorthosite Particle Size Distribution

2.2 Basalt (Merriam Crater)

Batch dates: 08/01/2023-Present

Description: Mafic igneous rock containing plagioclase, pyroxene, olivine, and volcanic glass

Source: Merriam Crater Basalt sourced from the Merriam Crater near Flagstaff, AZ. This is the same source as JSC-1A**.**

Figure 6. Photo of Basalt.

2.2.1 Chemistry from X-Ray Fluorescence

Table 3. Basalt (Glass-Rich) - Approximate Bulk Chemistry

Compound	Concentration (wt %)
SiO_2	47.71
TiO_2	1.59
Al_2O_3	15.02
Fe_2O_3	10.79
MnO	0.19
MgO	9.39
CaO	9.9
Na_2O	2.7
K_2O	0.82
P_2O_5	0.66
Total	98.77

2.2.2 Basalt Particle Size Analysis

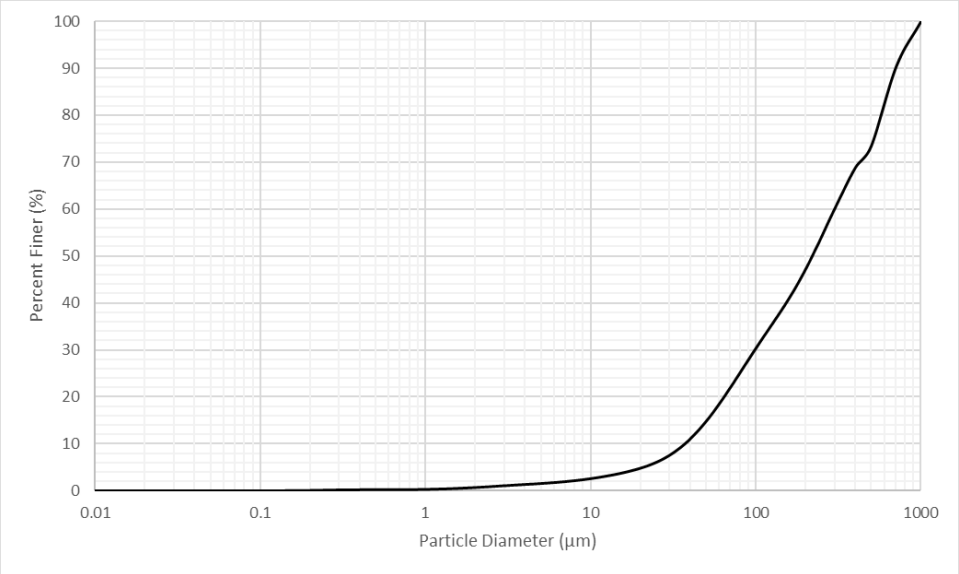

Figure 7. Basalt Particle Size Distribution

2.3 Basalt (Butler)

Batch dates: 06/01/2021-07/31/2023

Description: Mafic igneous rock containing plagioclase, pyroxene, olivine, and volcanic glass

Source: Butler Arts Basalt

Figure 8. Photo of Basalt.

2.3.1 Chemistry from X-Ray Fluorescence

Table 4. Basalt (Glass-Rich) - Approximate Bulk Chemistry

Compound	Concentration (wt %)
SiO_2	45.7
TiO_2	2.5
Al_2O_3	15.5
Fe_2O_3	10.4
MnO	0.2
MgO	8.8
CaO	9.3
Na_2O	3.6
K_2O	2.1
P_2O_5	0.6
Total	98.7

2.3.2 Basalt Particle Size Analysis

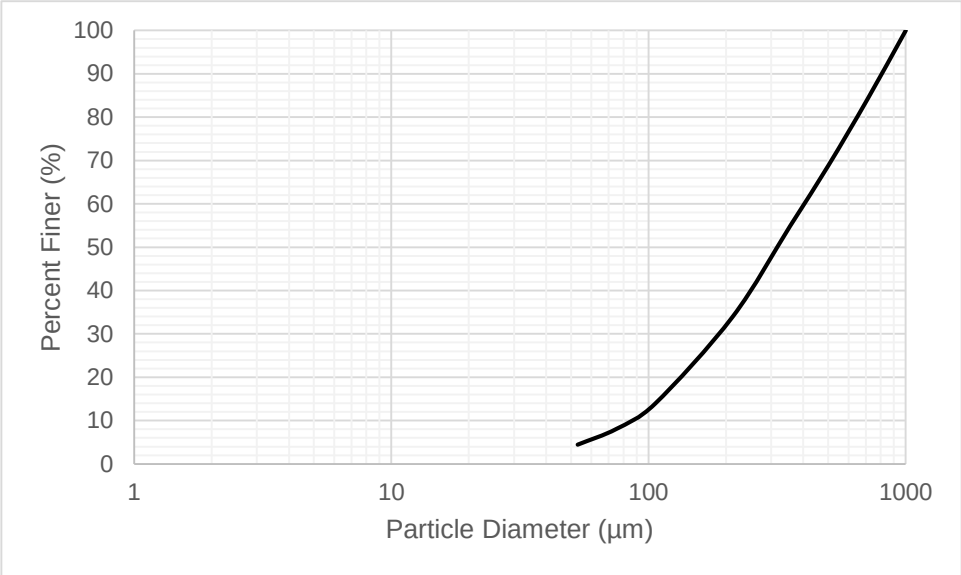

Figure 9. Basalt Particle Size Distribution

2.4 Basalt (Pebble Junction)

Batch dates: Before 06/01/2021

Description: Mafic igneous rock containing plagioclase, pyroxene, olivine, and volcanic glass

Source: Pebble Junction

Figure 10. Photo of Basalt.

2.4.1 Chemistry from X-Ray Fluorescence

Table 5. Basalt (Glass-Rich) - Approximate Bulk Chemistry

Compound	Concentration (wt %)
SiO_2	52.7
TiO_2	1.3
Al_2O_3	16.5
Fe_2O_3	9.1
MnO	0.1
MgO	5.8
CaO	8.2
Na_2O	3.8
K_2O	1.3
P_2O_5	0.4
Total	99.2

2.5 Bronzite

• Description: Pyroxene-group mineral

• Source: Stillwater Mine

• Idealized Formula: $(Mg,Fe)_3SiO_3$

Notes: Major phase confirmed by XRD analysis (Figure 12, Table 6). The XRF results (Table 7) are consistent with the expected composition of Bronzite.

Figure 11. Photo of Bronzite.

2.5.1 X-Ray Diffraction Pattern

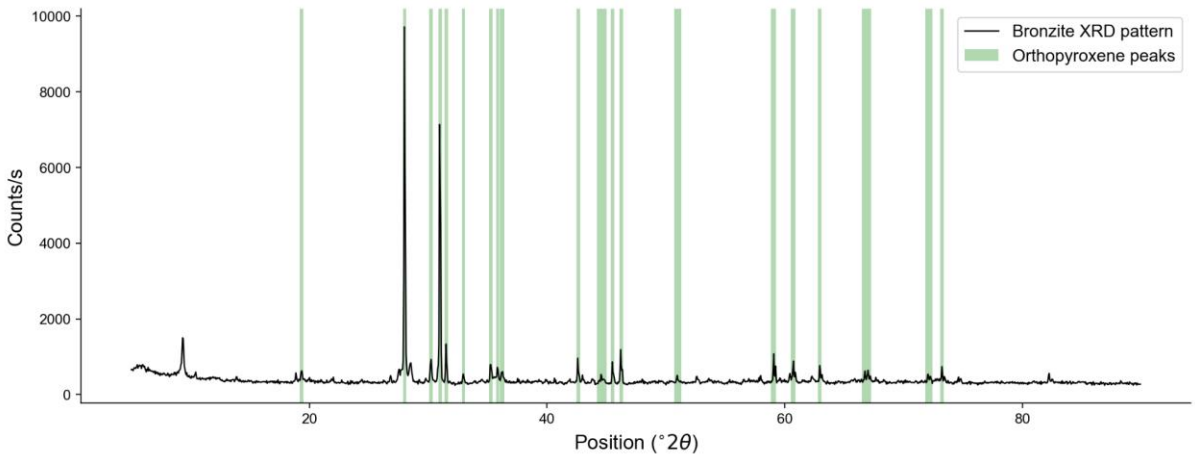

Figure 12. XRD Pattern for Bronzite Sample.

Table 6. Bronzite - XRD Pattern Peaks

Position (°2θ)	*Relative Intensity (%)*	*d-spacing (Å)*	*Matched By*
5.77	5.0	15.31	
9.37	15.2	9.44	
19.35	4.1	4.59	Orthopyroxene $(Mg_{2.83}Fe_{1.17})Si_4O_{12}$
28.02	100.0	3.18	Orthopyroxene $(Mg_{2.83}Fe_{1.17})Si_4O_{12}$
28.52	7.2	3.13	
30.23	8.0	2.96	Orthopyroxene $(Mg_{2.83}Fe_{1.17})Si_4O_{12}$
30.99	80.2	2.89	Orthopyroxene $(Mg_{2.83}Fe_{1.17})Si_4O_{12}$
31.52	10.5	2.84	Orthopyroxene $(Mg_{2.83}Fe_{1.17})Si_4O_{12}$
32.97	2.8	2.72	Orthopyroxene $(Mg_{2.83}Fe_{1.17})Si_4O_{12}$
35.27	6.3	2.54	Orthopyroxene $(Mg_{2.83}Fe_{1.17})Si_4O_{12}$
35.85	5.3	2.50	Orthopyroxene $(Mg_{2.83}Fe_{1.17})Si_4O_{12}$
36.22	3.9	2.48	Orthopyroxene $(Mg_{2.83}Fe_{1.17})Si_4O_{12}$
42.62	5.4	2.12	Orthopyroxene $(Mg_{2.83}Fe_{1.17})Si_4O_{12}$
44.61	1.8	2.03	Orthopyroxene $(Mg_{2.83}Fe_{1.17})Si_4O_{12}$
45.53	4.6	1.99	Orthopyroxene $(Mg_{2.83}Fe_{1.17})Si_4O_{12}$
46.22	7.9	1.96	Orthopyroxene $(Mg_{2.83}Fe_{1.17})Si_4O_{12}$
51.00	1.4	1.79	Orthopyroxene $(Mg_{2.83}Fe_{1.17})Si_4O_{12}$
59.04	7.0	1.56	Orthopyroxene $(Mg_{2.83}Fe_{1.17})Si_4O_{12}$
60.69	6.3	1.53	Orthopyroxene $(Mg_{2.83}Fe_{1.17})Si_4O_{12}$
62.95	6.1	1.48	Orthopyroxene $(Mg_{2.83}Fe_{1.17})Si_4O_{12}$
66.87	2.2	1.40	Orthopyroxene $(Mg_{2.83}Fe_{1.17})Si_4O_{12}$
72.13	2.1	1.31	Orthopyroxene $(Mg_{2.83}Fe_{1.17})Si_4O_{12}$
73.21	4.9	1.29	Orthopyroxene $(Mg_{2.83}Fe_{1.17})Si_4O_{12}$
74.70	1.3	1.27	
82.22	3.6	1.17	

Peak match citation: PDF 98-018-8072 in Gates-Rector and Blanton (2019)

2.5.2 Chemistry from X-Ray Fluorescence

Table 7. Bronzite - Bulk Chemistry

Compound	*Concentration (wt%)*
MgO	27.5
Al_2O_3	3.3
SiO_2	45.0
P_2O_5	1.1
SO_3	0.1
Cl	0.2
K_2O	0.1
CaO	4.8
TiO_2	0.3
Cr_2O_3	0.7
MnO	0.3
Fe_2O_3	16.5
NiO	0.1
Total	99.9

2.5.3 FTIR Spectroscopy

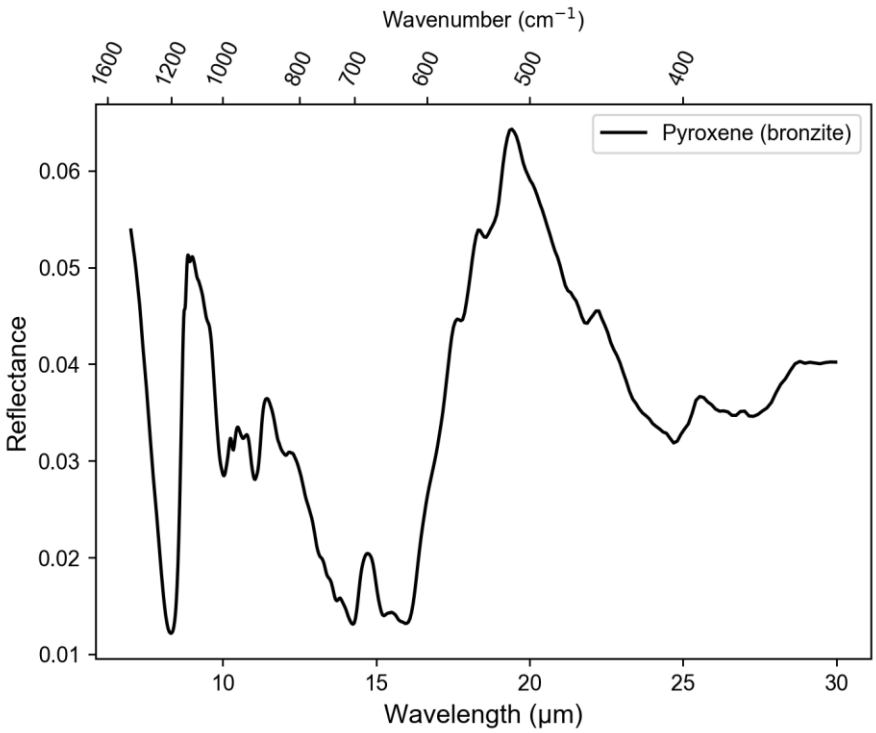

Figure 13. Bronzite FTIR Spectroscopy

2.5.4 VIS NIR Spectroscopy

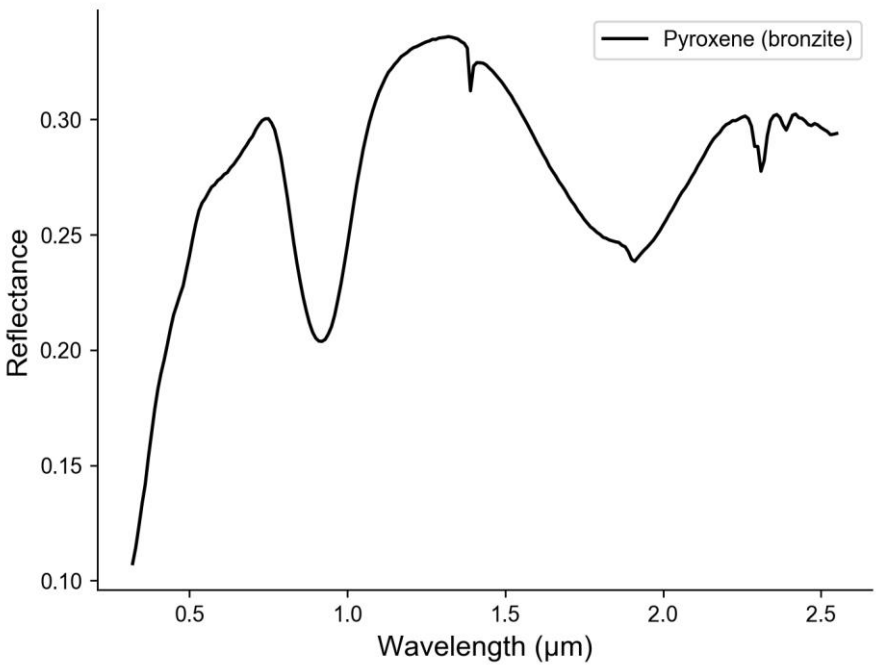

Figure 14. Bronzite VIS NIR Spectroscopy

2.5.5 Particle Size Analysis

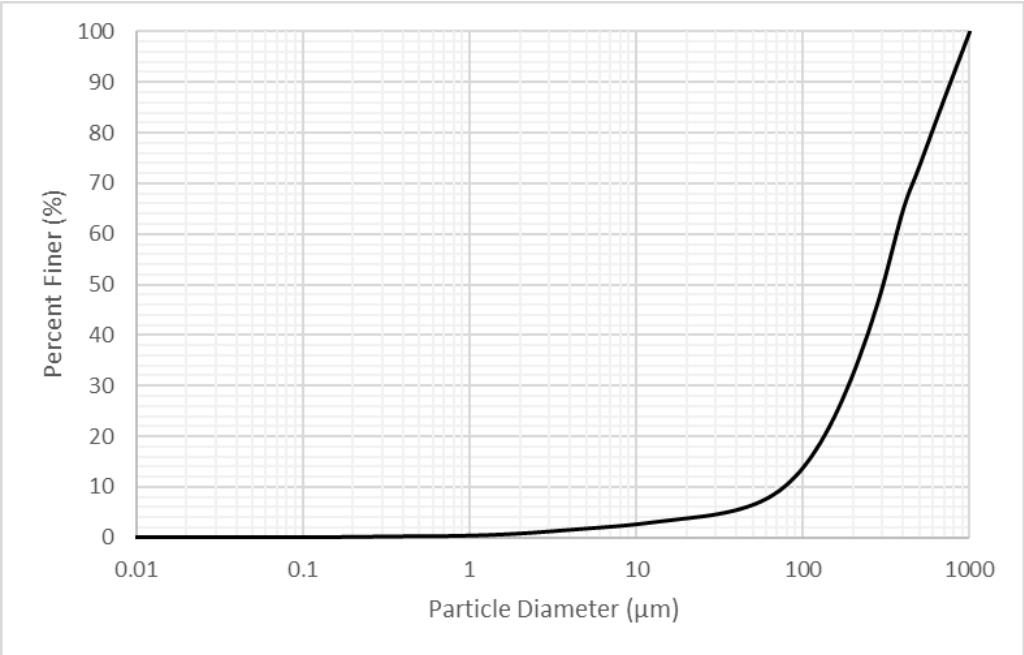

Figure 15. Bronzite Particle Size Distribution

2.6 Epsomite

• Description: Amorphous Magnesium Sulfate

• Source: Kali EPSOTop

• Idealized Formula: MgSO4·7H2O

Notes: Epsomite is water soluble

Figure 16. Photo of Epsomite

2.6.1 Bulk Chemistry from Source

Table 8. Epsomite - Bulk Chemistry

Compound	Concentration (%)
MgO	16
SO_4	32.5
H_2O	50.9
Total	99.4

2.7 Ferrihydrite

- Description: Hydrous ferric oxyhydroxide mineral
- Source: Kolar Labs High Capacity Granular Ferric Oxide (HC GFO)
- Idealized Formula: $(Fe^{3+})_2O_3 \cdot 0.5H_2O$

Notes: XRD analysis (Figure 18, Table 9) confirms the primary phase is two-line ferrihydrite (2LFh), so named for its two XRD peaks (Vaughan et al., 2012); the more structured form of ferrihydrite shows 6 XRD peaks (Figure 19). Only the strongest of the two peaks, at 2θ = 35.8122°, was identified by algorithm, although the expected secondary peak at 2θ = 63.50° is identifiable by eye. XRF analysis (Table 10). confirms > 92% Fe_2O_3.

Figure 17. Photo of Ferrihydrite.

2.7.1 X-Ray Diffraction Pattern

Table 9. Ferrihydrite - XRD Pattern Peaks

Position (°2θ)	*Relative Intensity (%)*	*d-spacing (Å)*	*Matched By*
35.8122	100	2.50538	Two-line ferrihydrite
63.50	– (ID'd by eye)	– (ID'd by eye)	Two-line ferrihydrite

Peak match citation: Vaughan et al. (2012)

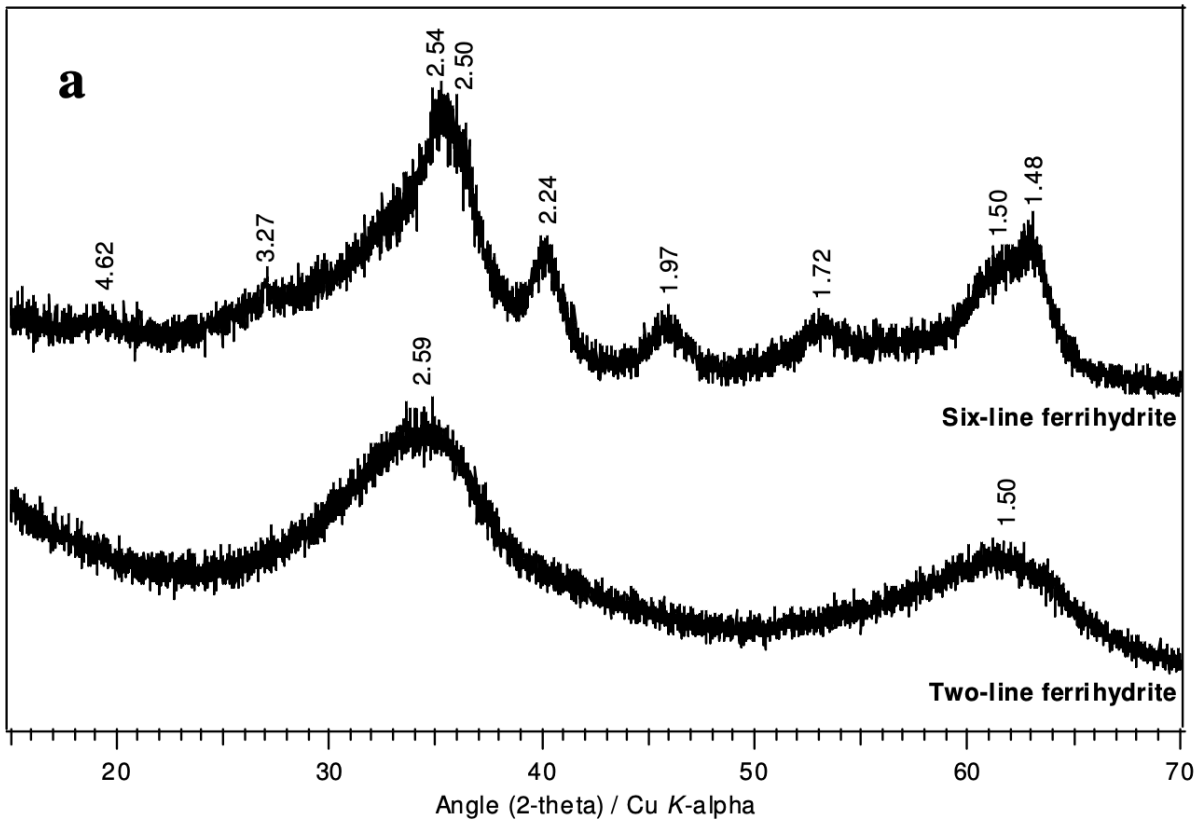

Figure 18. From Vaughan et al. (2012): powder XRD patterns for both two- and six-line ferrihydrite.

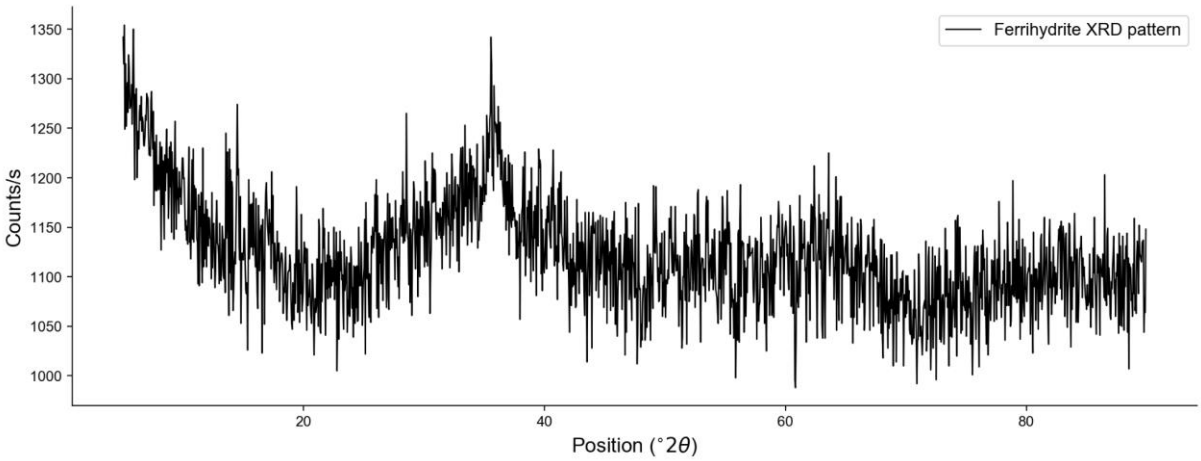

Figure 19. XRD pattern for ferrihydrite sample.

2.7.2 Chemistry from X-Ray Fluorescence

Table 10. Ferrihydrite - Bulk Chemistry

Compound	*Concentration (wt%)*
MgO	5.3
Al_2O_3	0.3
P_2O_5	0.7
SO_3	0.2
Cl	0.1
CaO	0.3
Cr_2O_3	0.1
MnO	0.2
Fe_2O_3	92.6
NiO	0.1
Rb_2O	0.0
HfO_2	<0.1
Total	99.9

2.7.3 FTIR Spectroscopy

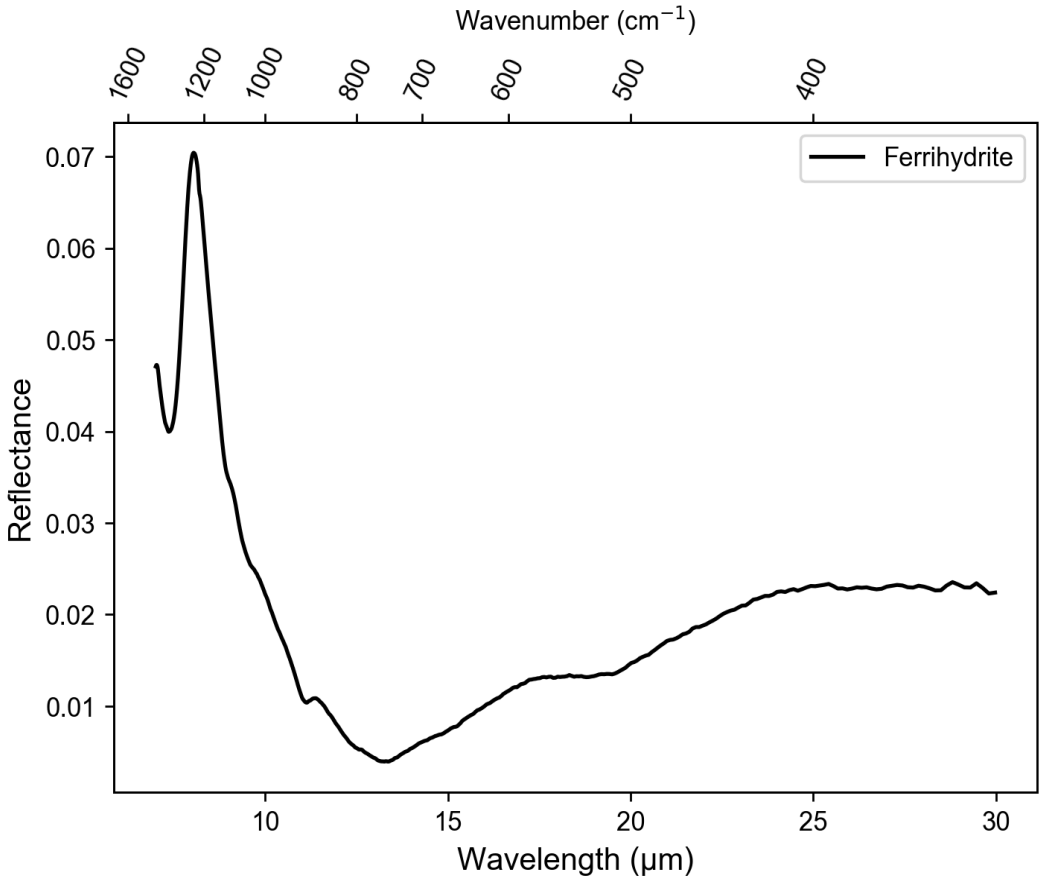

Figure 20. Ferrihydrite FTIR Spectroscopy

2.7.4 VIS NIR Spectroscopy

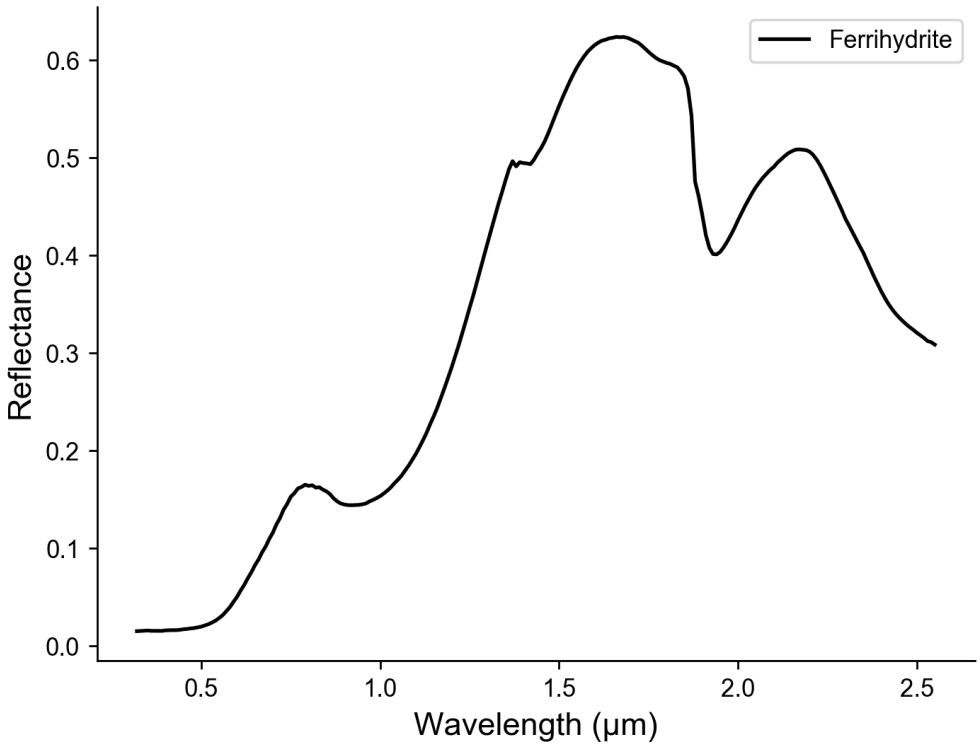

Figure 21. Ferrihydrite FTIR Spectroscopy

2.7.5 Particle Size Analysis

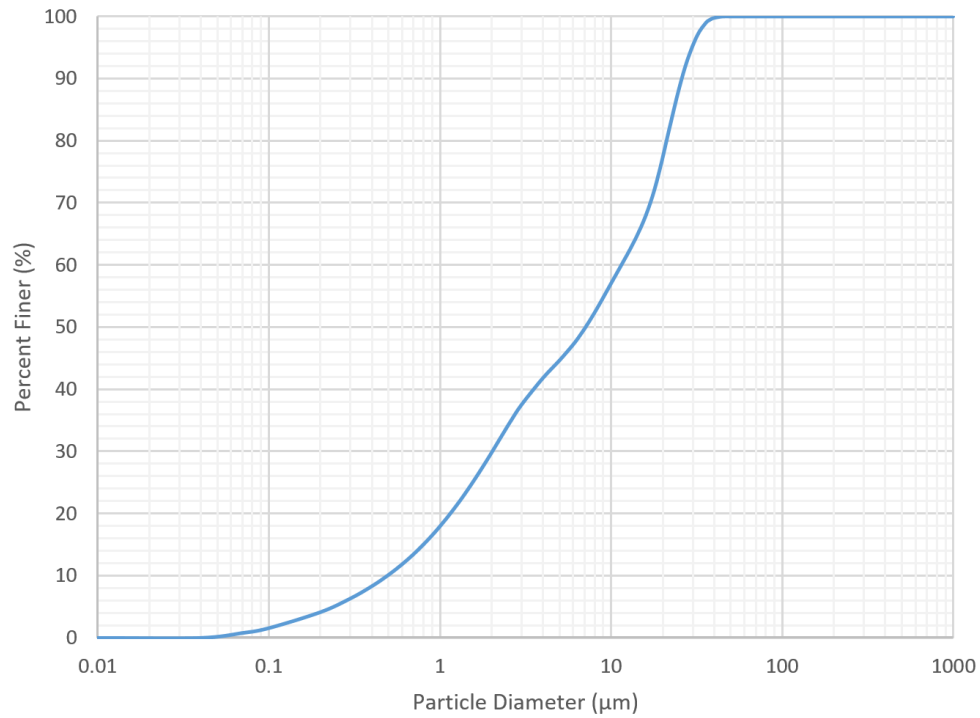

Figure 22. Ferrihydrite Particle Size Distribution

2.8 Gypsum

- Description: Calcium sulfate
- Source: –
- Idealized Formula: $CaSO_4 \cdot 2H_2O$

Notes Major phase confirmed by XRD analysis (Figure 24, Table 11). Additional peaks indicate the presence of a minor contaminant phase. XRF analysis (Table 12) confirms CaO and SO_3 are the major compounds present.

Figure 23. Photo of Gypsum.

2.8.1 X-Ray Diffraction Pattern

Table 11. Gypsum- XRD Pattern Peaks

Position (°2θ)	*Relative Intensity (%)*	*d-spacing (Å)*	*Matched By*
6.18	1.0	14.29	
8.72	13.9	10.14	
9.42	1.4	9.38	
10.46	1.2	8.46	
11.59	100.0	7.63	Gypsum
12.43	1.1	7.12	
17.52	0.5	5.06	
18.70	0.7	4.75	
20.69	8.6	4.29	Gypsum
23.36	11.8	3.81	Gypsum
24.06	0.1	3.70	
25.07	0.8	3.55	
26.43	5.1	3.37	
27.94	0.6	3.19	
28.55	0.7	3.13	
29.09	8.2	3.07	Gypsum
29.42	0.3	3.04	
30.93	3.8	2.89	Gypsum
31.50	0.2	2.84	
32.03	0.2	2.79	Gypsum
33.34	1.0	2.69	Gypsum
34.50	0.5	2.60	Gypsum
35.44	0.5	2.53	Gypsum
35.95	0.2	2.50	Gypsum
36.60	0.7	2.46	Gypsum
37.38	0.2	2.41	Gypsum
39.48	0.1	2.28	Gypsum
40.62	0.7	2.22	Gypsum
42.15	0.1	2.14	Gypsum
43.33	0.6	2.09	Gypsum
43.62	0.3	2.07	Gypsum
44.18	0.3	2.05	Gypsum
44.82	0.6	2.02	
45.49	0.4	1.99	Gypsum
47.82	1.2	1.90	Gypsum
48.36	0.4	1.88	Gypsum
48.72	0.2	1.87	Gypsum
50.30	0.7	1.81	Gypsum
51.32	0.5	1.78	Gypsum
53.58	0.1	1.71	Gypsum
54.43	0.1	1.69	Gypsum
55.10	0.3	1.67	Gypsum
56.70	0.8	1.62	Gypsum
58.10	0.2	1.59	Gypsum
60.34	0.1	1.53	Gypsum
63.67	0.2	1.46	Gypsum
64.57	0.1	1.44	Gypsum
65.86	0.1	1.42	Gypsum
67.33	0.2	1.39	
68.62	0.5	1.37	Gypsum
70.60	0.3	1.33	Gypsum
71.15	0.2	1.33	Gypsum
74.04	0.1	1.28	Gypsum
74.93	0.1	1.27	Gypsum
76.45	0.2	1.25	Gypsum
76.93	0.1	1.24	
79.58	0.1	1.20	
83.25	0.2	1.16	
84.94	0.1	1.14	
85.90	0.1	1.13	

Peak match citation: PDF 00-033-0311 in Gates-Rector and Blanton (2019)

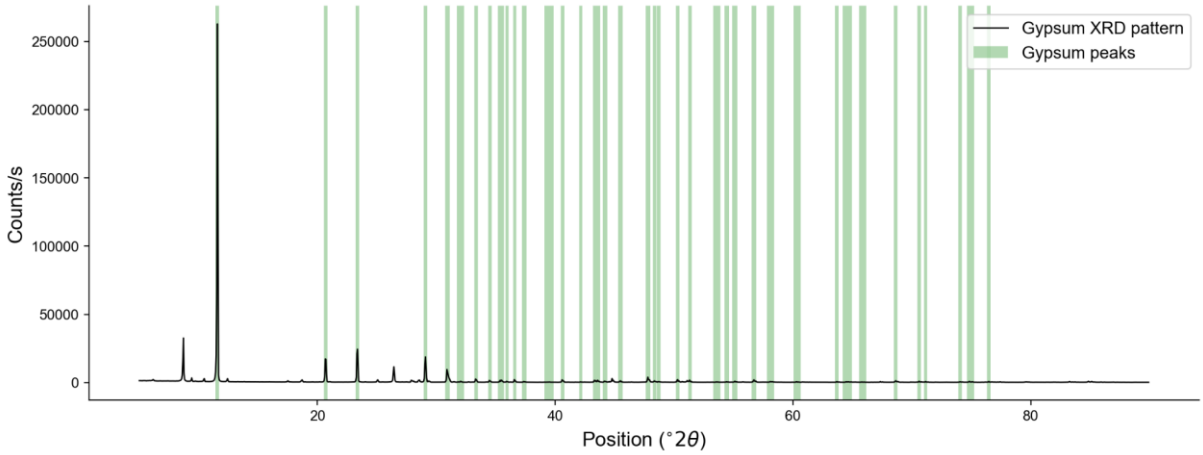

Figure 24. XRD pattern for gypsum sample shown with a reference pattern (Schofield et al., 1996).

2.8.2 Chemistry from X-Ray Fluorescence

Table 12. Gypsum - Bulk Chemistry

Compound	*Concentration (wt%)*
MgO	4.8
Al_2O_3	1.9
SiO_2	4.2
P_2O_5	0.7
SO_3	45.0
Cl	0.1
K_2O	0.5
CaO	41.9
TiO_2	0.2
Fe_2O_3	0.5
SrO	0.2
Total	100.0

2.8.3 FTIR Spectroscopy

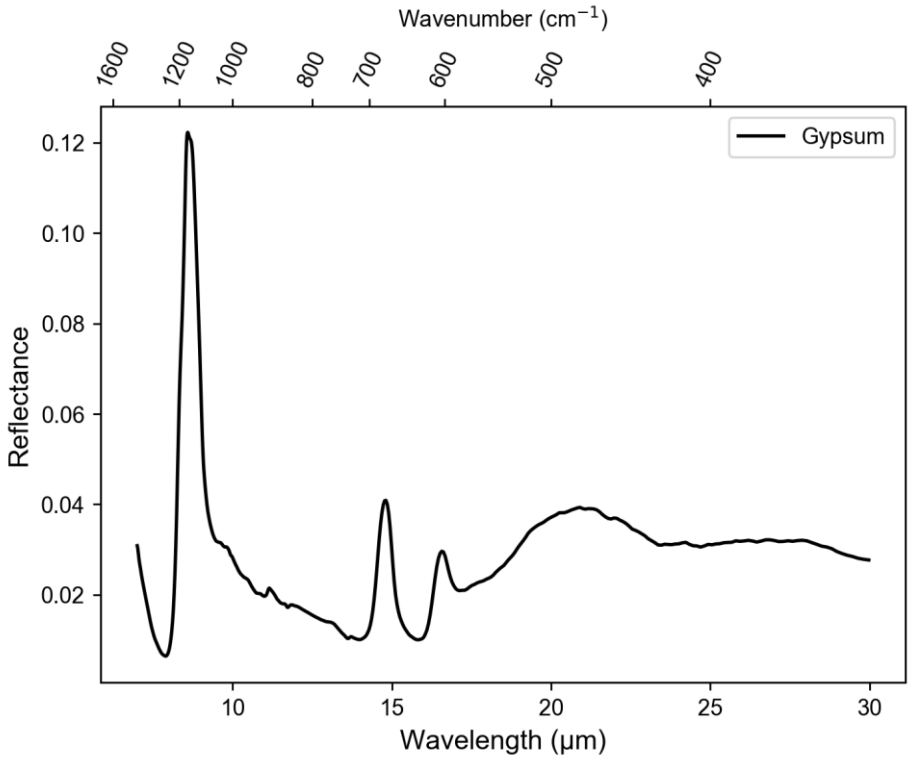

Figure 25. Gypsum FTIR Spectroscopy

2.8.4 VIS NIR Spectroscopy

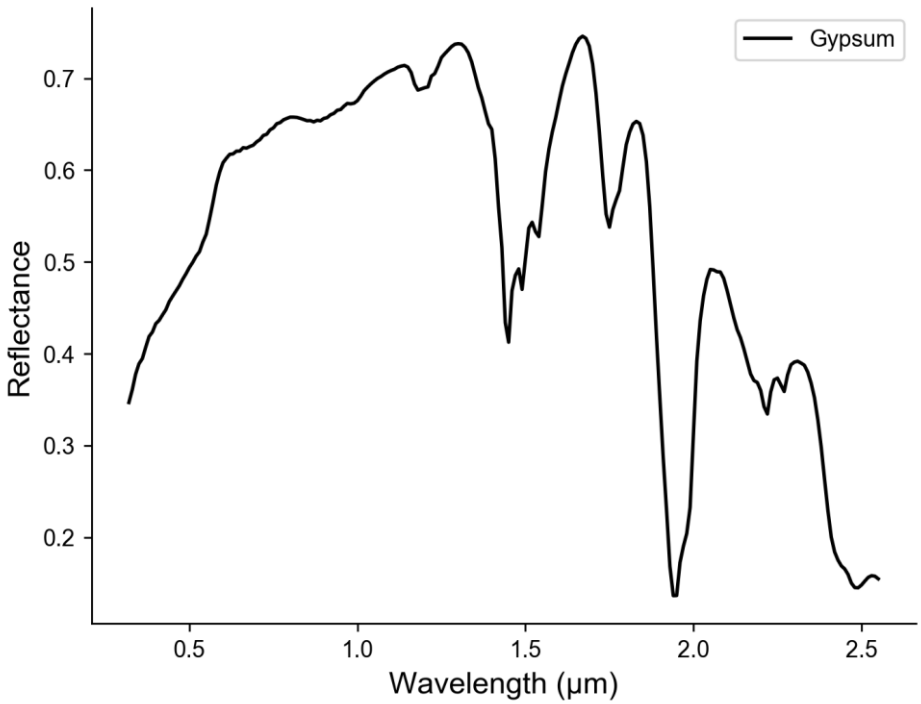

Figure 26. Gypsum FTIR Spectroscopy

2.8.5 Particle Size Analysis

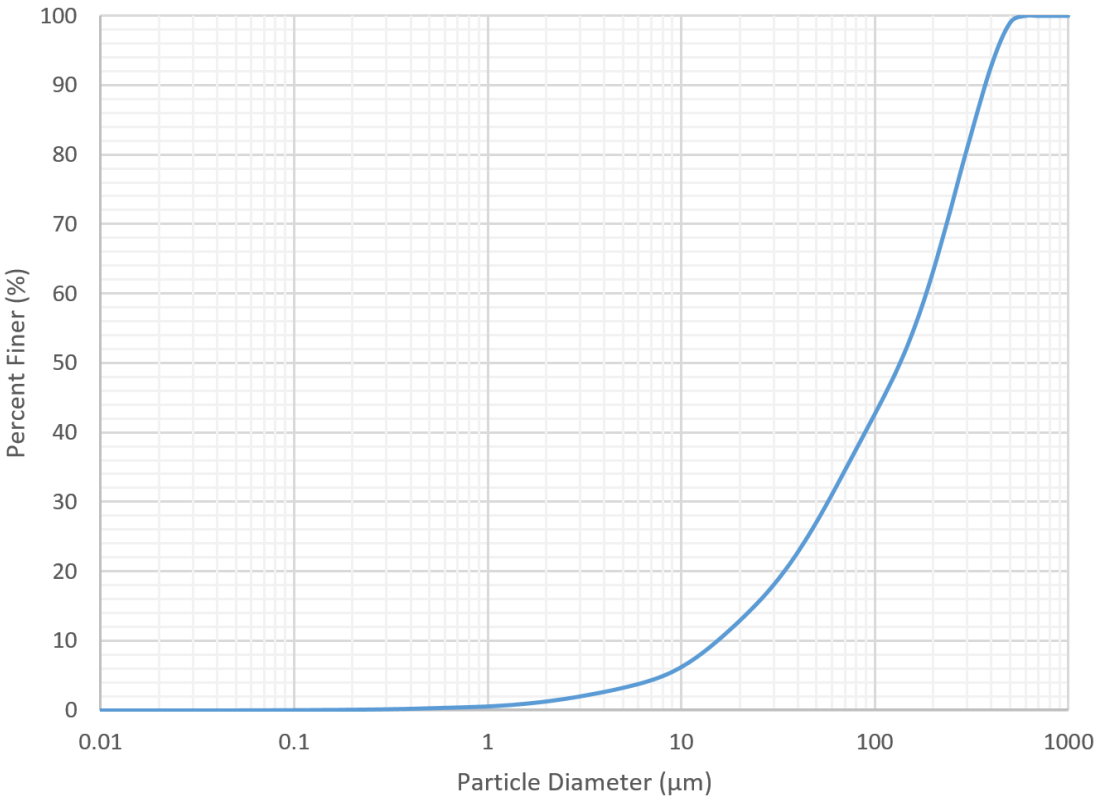

Figure 27. Gypsum Particle Size Distribution

2.9 Hematite

• Description: Iron oxide

• Source: Alpha Chemicals Red Iron Oxide

• Idealized Formula:Fe_2O_3

• Also called: Iron(III) oxide, red iron oxide

Notes Major phase confirmed by XRD analysis (Figure 29, Table 13). Additional peaks indicate the presence of a minor contaminant phase. XRF analysis (Table 14) shows 87.3 wt% iron oxide with an excess of SiO_2 (6.7 wt%) and Al_2O_3 (3.0 wt%), suggesting the presence of an aluminum silicate.

Figure 28. Photo of Hematite

2.9.1 X-Ray Diffraction Pattern

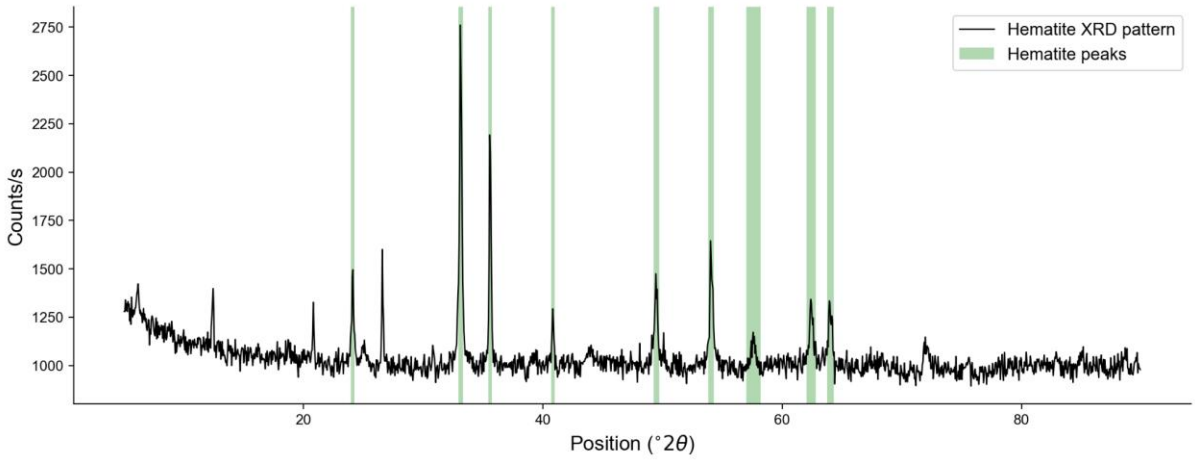

Figure 29. XRD Pattern for Hematite Sample

Table 13. Hematite - XRD Pattern Peaks

Position (°2θ)	*Relative Intensity (%)*	*d-spacing (Å)*	*Matched By*
5.51	15.9	16.04	
12.42	19.4	7.12	
20.84	17.2	4.26	
24.11	30.8	3.69	Hematite
26.60	32.5	3.35	
33.14	100.0	2.70	Hematite
35.60	70.5	2.52	Hematite
40.85	16.9	2.21	Hematite
49.48	24.1	1.84	Hematite
54.04	37.3	1.70	Hematite
57.59	8.6	1.60	Hematite
62.43	19.8	1.49	Hematite
64.03	17.3	1.45	Hematite

Peak match citation: PDF 00-024-0072 in Gates-Rector and Blanton (2019)

2.9.2 Chemistry from X-Ray Fluorescence

Table 14. Hematite - Bulk Chemistry

Compound	*Concentration (wt%)*
Al_2O_3	3.0
SiO_2	6.7
P_2O_5	0.8
SO_3	0.1
Cl	0.1
K_2O	0.3
CaO	0.8
TiO_2	0.2
MnO	0.5
Fe_2O_3	87.3
NiO	0.1
HfO_2	< 0.1
Total	99.9

2.9.3 FTIR Spectroscopy

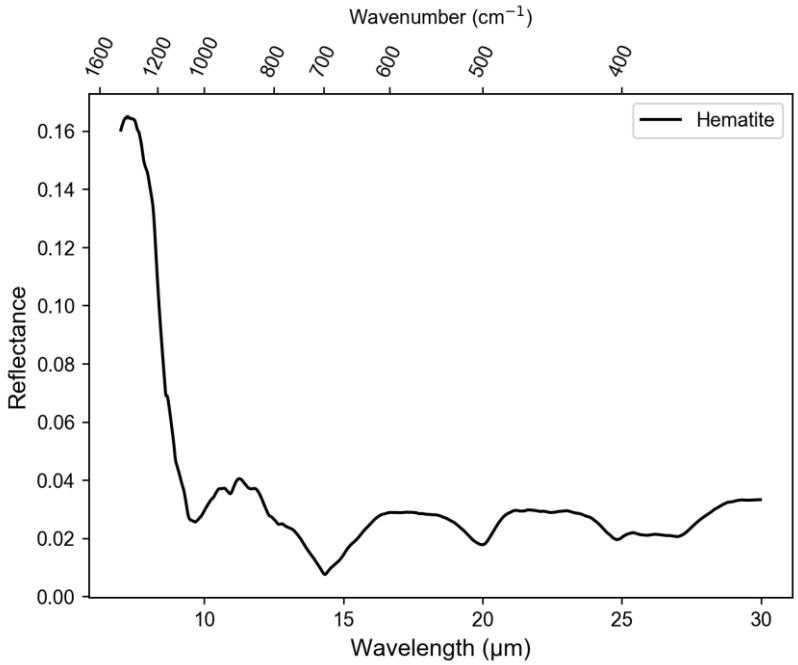

Figure 30. Hematite FTIR Spectroscopy

2.9.4 VIS NIR Spectroscopy

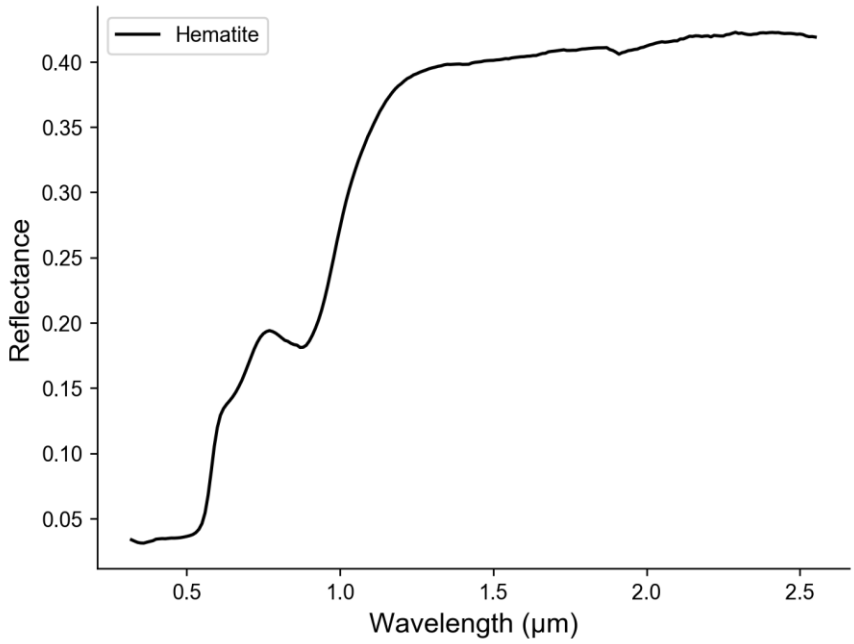

Figure 31. Hematite VIS NIR Spectroscopy

2.9.5 Particle Size Analysis

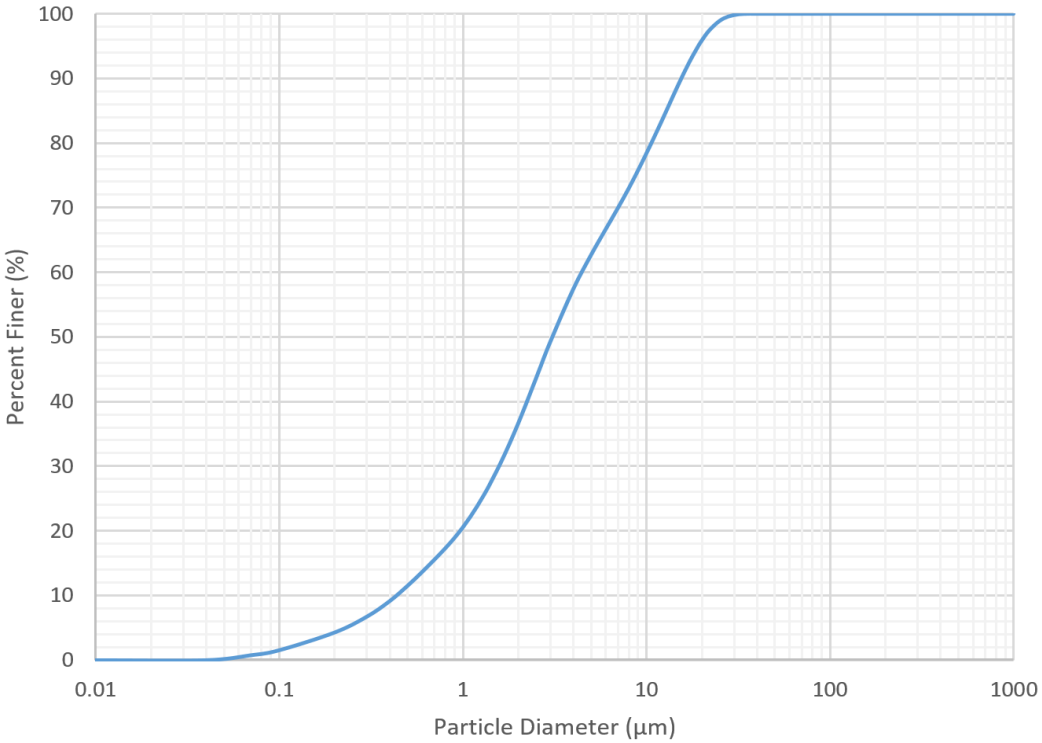

Figure 32. Hematite Particle Size Distribution

2.10 Hydrated Silica

• Description:

• Source: Diatomaceous Earth

• Idealized: SiO^2

• Also called: Hydrated Silica

Notes: Diatomaceous Earth is produced by microorganisms

Figure 33. Photo of Hydrated Silica

2.10.2 Chemistry from Supplier

Table 15. Hydrated Silica - Bulk Chemistry from Supplier

Compound	Concentration (%)
SiO^2	100.0%
Total	100.0%

2.10.3 Particle Size Analysis

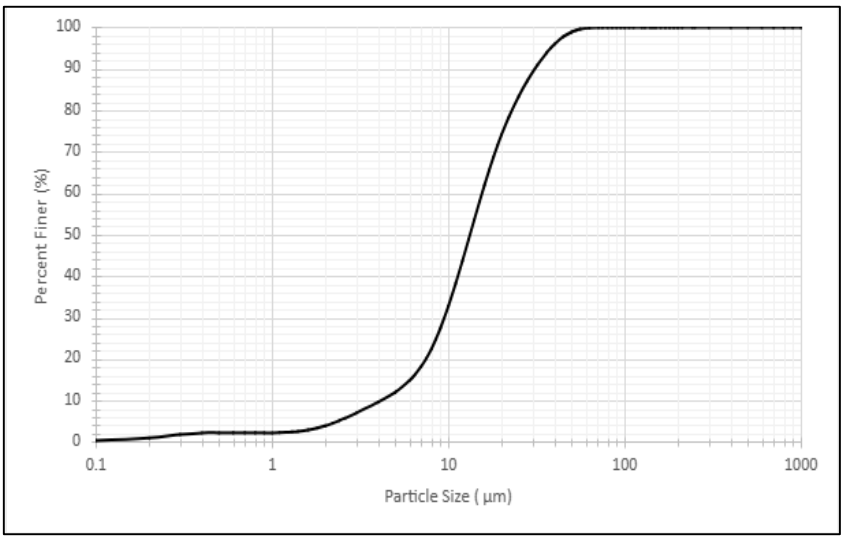

Figure 34. Hydrated Silica Particle Size Distribution

2.11 Magnesite

• Description: Magnesium carbonate

• Source: Reade

• Idealized Formula: $MgCO_3$

Notes Major phase confirmed by XRD analysis (Table 16, Figure 36). The MCF's XRF analyzer cannot detect carbon. The XRF data (Table 17) are otherwise consistent with magnesite as the main phase, with 69.3% MgO. There is some evidence of contamination from an aluminum silicate phase in the XRF data, but their relative concentrations would be lower if carbon could be detected and were included in the bulk chemistry quantification.

Figure 35. Photo of Magnesite

2.11.1 X-Ray Diffraction Pattern

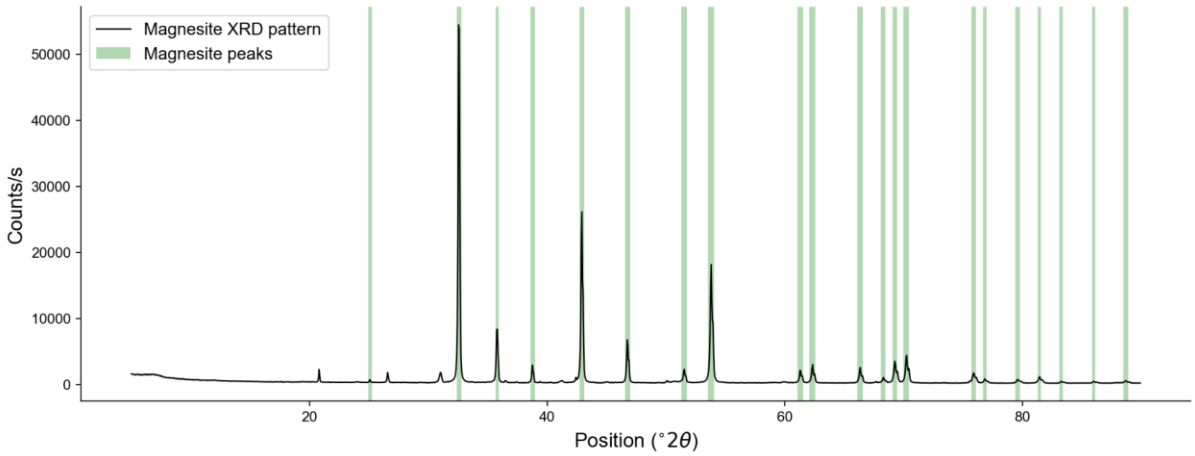

Figure 36. XRD Pattern for Magnesite Sample

Table 16. Magnesite - XRD Pattern Peaks

Position (°2θ)	*Relative Intensity (%)*	*d-spacing (Å)*	*Matched By*
7.08	1.5	12.48	
20.83	3.3	4.27	
25.09	0.8	3.55	Magnesite
26.60	2.6	3.35	
31.04	2.8	2.88	
32.59	100.0	2.75	Magnesite
35.80	14.5	2.51	Magnesite
36.52	0.5	2.46	
38.79	4.4	2.32	Magnesite
41.23	0.6	2.19	
42.93	47.4	2.11	Magnesite
45.01	0.2	2.01	
46.77	11.0	1.94	Magnesite
51.54	3.7	1.77	Magnesite
53.79	30.8	1.70	Magnesite
59.95	0.3	1.54	
61.29	3.6	1.51	Magnesite
62.30	4.8	1.49	Magnesite
66.32	4.1	1.41	Magnesite
68.27	1.4	1.37	Magnesite
69.24	5.6	1.36	Magnesite
70.21	7.4	1.34	Magnesite
75.86	2.7	1.25	Magnesite
76.81	1.1	1.24	Magnesite
79.58	1.0	1.20	Magnesite
81.41	1.8	1.18	Magnesite
83.25	0.4	1.16	Magnesite
85.97	0.5	1.13	Magnesite
88.68	0.6	1.10	Magnesite

Peak match citation: PDF 01-071-1534 in Gates-Rector and Blanton (2019)

2.11.2 Chemistry from X-Ray Fluorescence

Table 17. Magnesite - Bulk Chemistry

Compound	*Concentration (wt%)*
MgO	69.3
Al_2O_3	0.8
SiO_2	11.6
P_2O_5	2.8
SO_3	1.4
Cl	1.9
CaO	11.2
Cr_2O_3	0.1
MnO	0.1
Fe_2O_3	0.6
NiO	0.3
Total	100.0

2.11.3 FTIR Spectroscopy

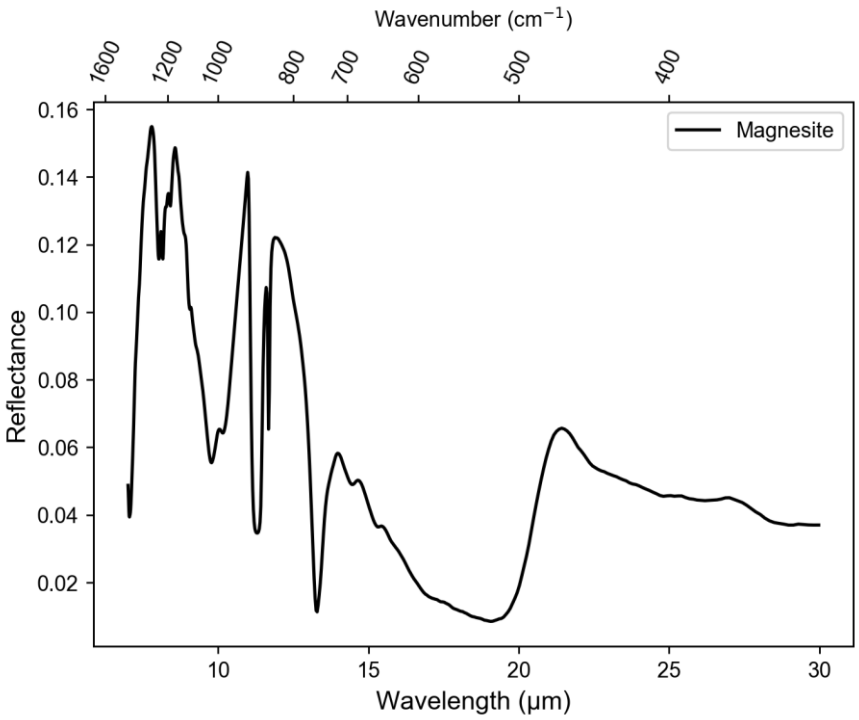

Figure 37. Magnesite FTIR Spectroscopy

2.11.4 VIS NIR Spectroscopy

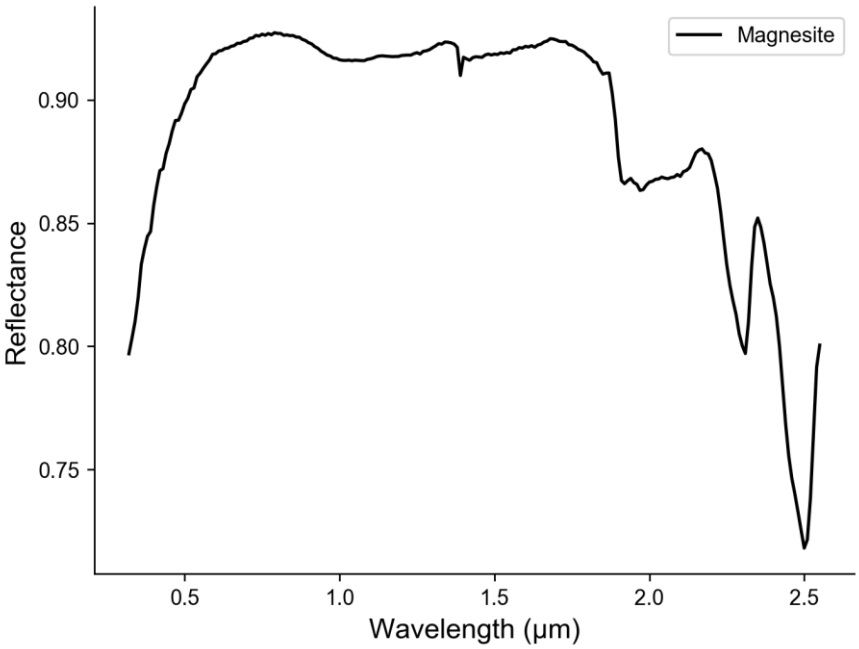

Figure 38. Magnesite VIS NIR Spectroscopy

2.11.5 Particle Size Analysis

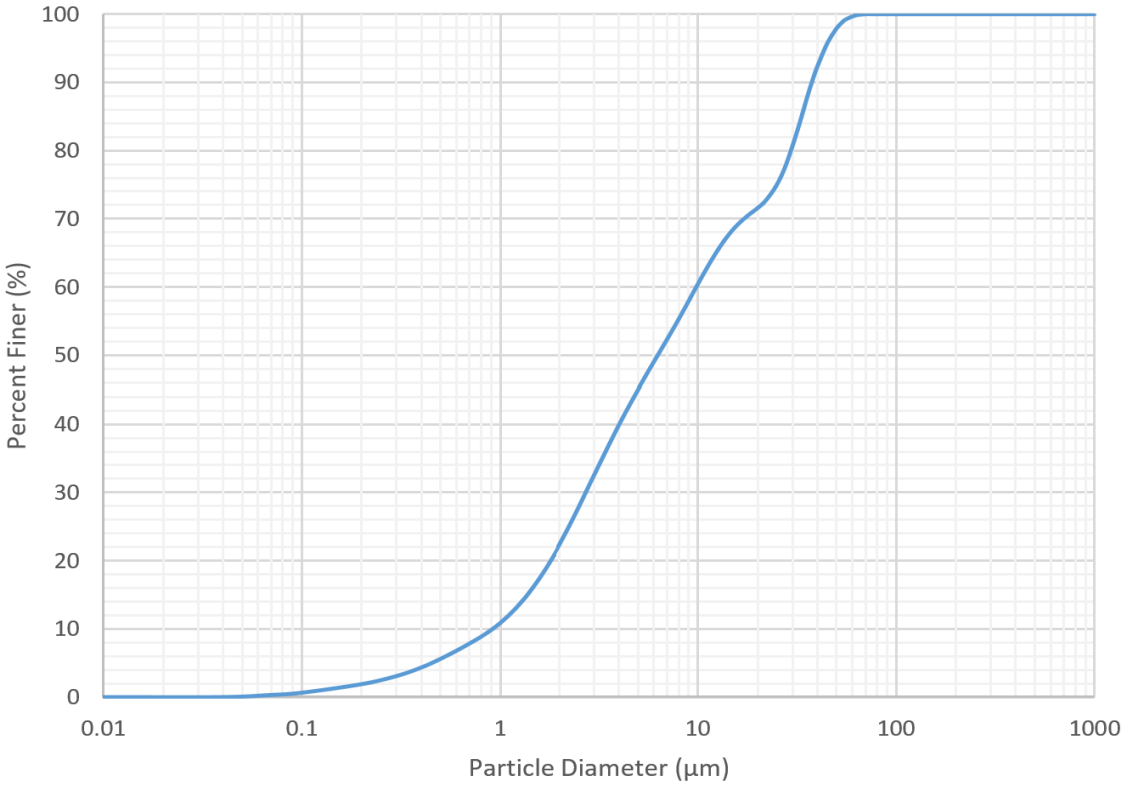

Figure 39. Magnesite Particle Size Distribution

2.12 Magnetite

• Description: Iron oxide

• Source: –

• Idealized Formula: Fe_3O_4

• Also called: Ferrous-ferric oxide

Notes XRD analysis (Table 18, Figure 41) confirms the major phase is magnetite. XRF analysis (Table 19) shows ~90% iron oxide content.

Figure 40. Photo of Magnetite

2.12.1 X-Ray Diffraction Pattern

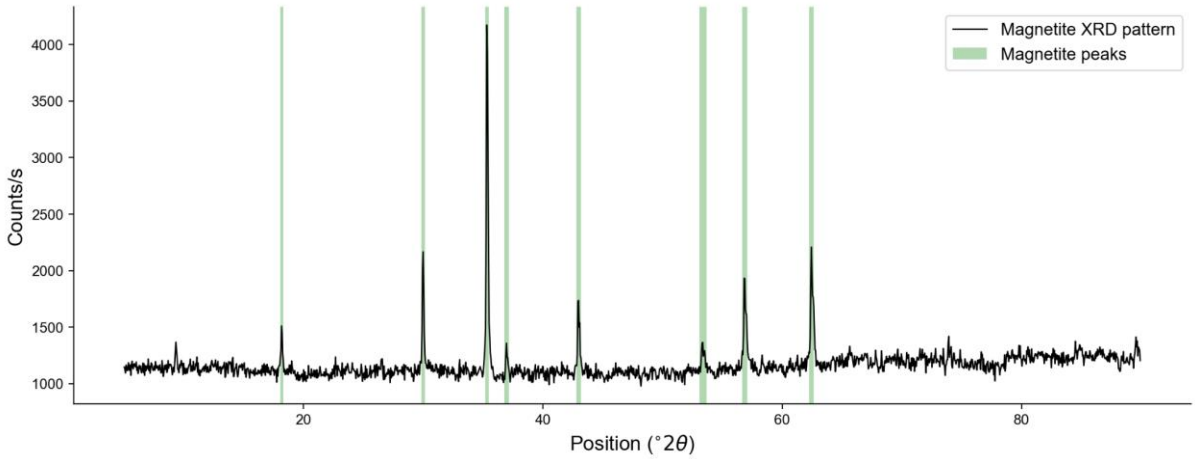

Figure 41. XRD Pattern for Magnetite Sample.

Table 18. Magnetite - XRD Pattern Peaks

Position (°2θ)	*Relative Intensity (%)*	*d-spacing (Å)*	*Matched By*
18.19	13.6	4.88	Magnetite
29.99	34.0	2.98	Magnetite
35.35	100.0	2.54	Magnetite
36.98	8.2	2.43	Magnetite
42.99	21.6	2.10	Magnetite
53.40	7.2	1.72	Magnetite
56.87	26.4	1.62	Magnetite
62.45	34.6	1.49	Magnetite
64.11	1.6	1.45	
80.43	2.0	1.19	

Peak match citation: PDF 01-071-6448 in Gates-Rector and Blanton (2019)

2.12.2 Chemistry from X-Ray Fluorescence

Table 19. Magnetite - Bulk Chemistry

Compound	*Concentration (wt%)*
MgO	4.2
Al_2O_3	0.1
SiO_2	2.9
P_2O_5	0.7
Cl	0.1
CaO	1.0
MnO	0.2
Fe_2O_3	90.7
Total	99.9

2.12.3 FTIR Spectroscopy

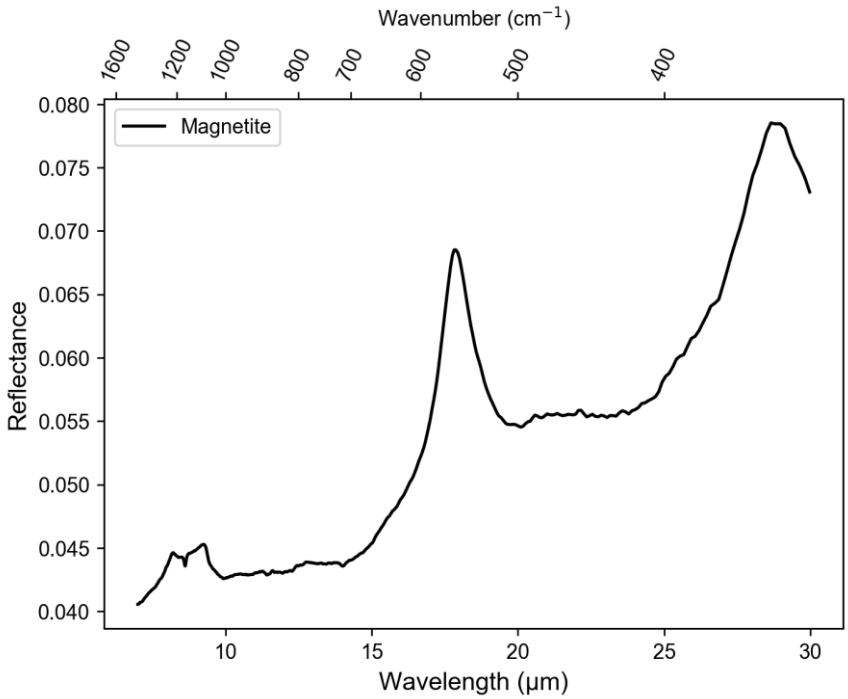

Figure 42. Magnetite FTIR Spectroscopy

2.12.4 VIS NIR Spectroscopy

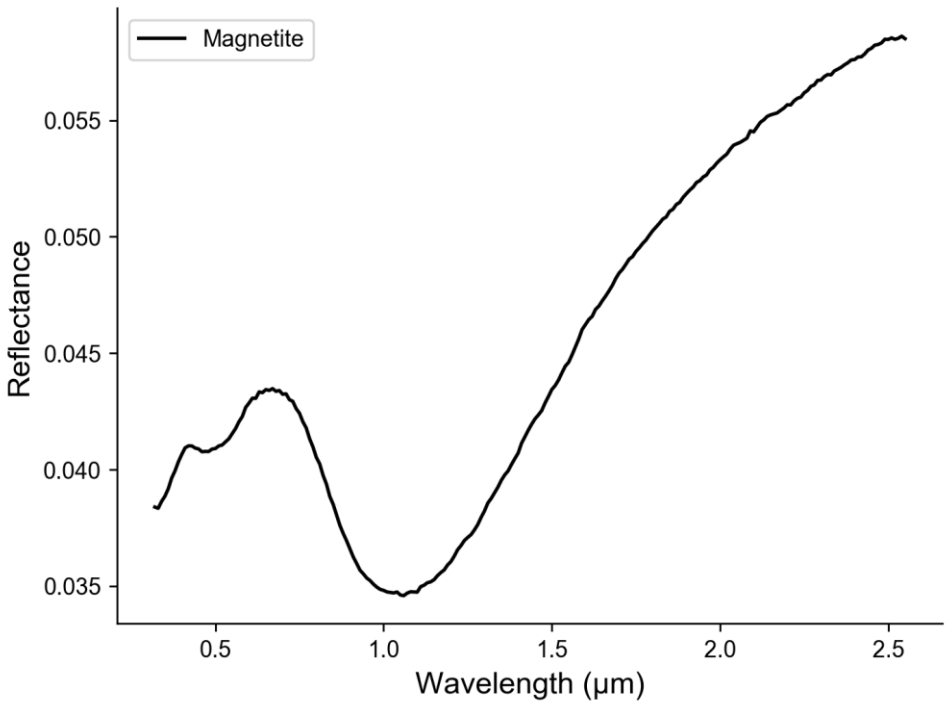

Figure 43. Magnetite VIS NIR Spectroscopy

2.12.5 Particle Size Analysis

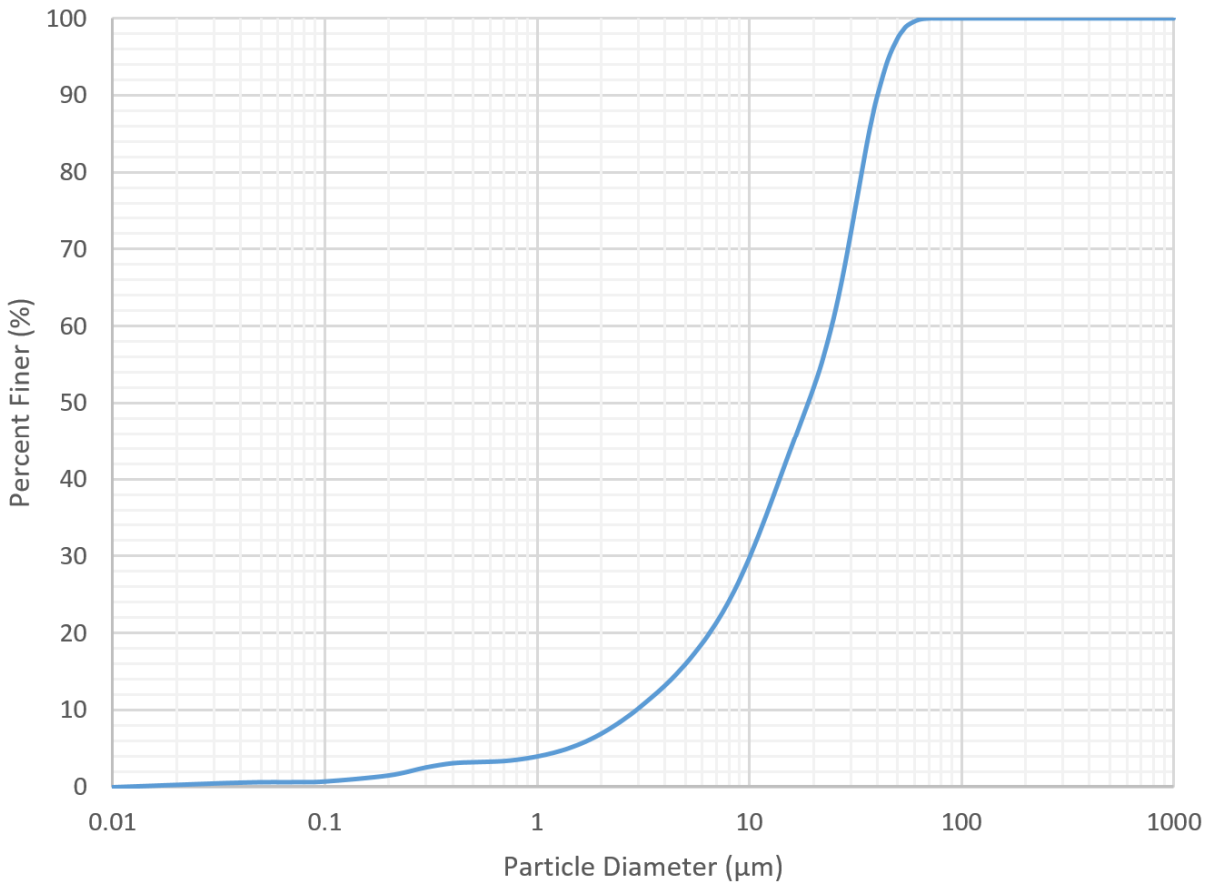

Figure 44. Magnetite Particle Size Distribution

2.13 Olivine

• Description: Nesosilicate mineral

• Source: United Western Supply

• Idealized Formula: $(Mg, Fe)_2SiO_4$

Notes Major phase confirmed by XRD analysis (Table 20, Figure 46). XRF analysis (Table 21) is consistent with a high fraction of Mg-rich olivine (forsterite).

Figure 45. Photo of Olivine

2.13.1 X-Ray Diffraction Pattern

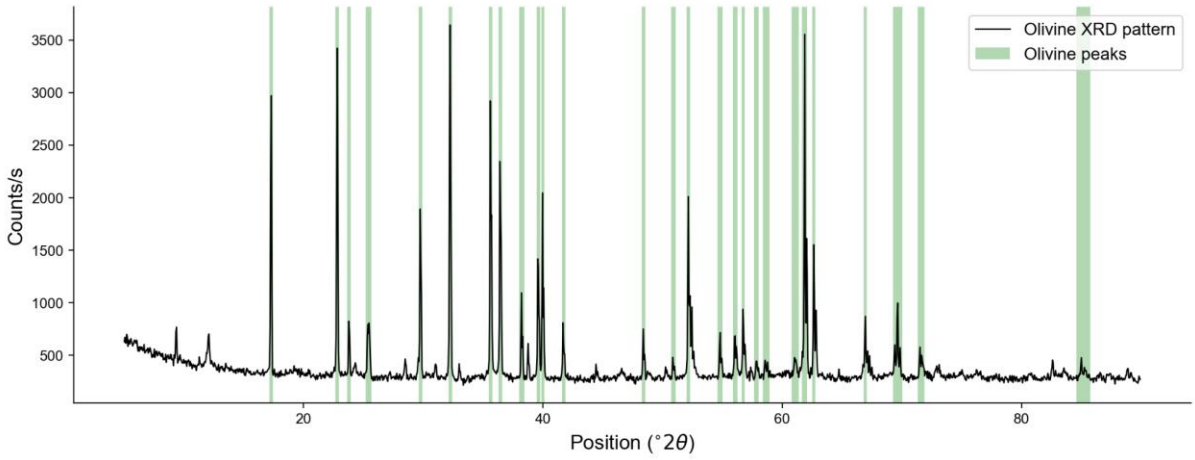

Figure 46. XRD pattern for Olivine sample

Table 20. Olivine - XRD Pattern Peaks

Position (°2θ)	*Relative Intensity (%)*	*d-spacing (Å)*	*Matched By*
9.37	9.6	9.44	
12.08	9.7	7.33	
17.30	74.2	5.13	Olivine $(Mg_{1.77}Fe_{0.23})SiO_4$)
22.82	100.0	3.90	Olivine $(Mg_{1.77}Fe_{0.23})SiO_4$)
23.82	15.6	3.74	Olivine $(Mg_{1.77}Fe_{0.23})SiO_4$)
25.43	14.0	3.50	Olivine $(Mg_{1.77}Fe_{0.23})SiO_4$)
28.50	5.5	3.13	
29.78	41.5	3.00	Olivine $(Mg_{1.77}Fe_{0.23})SiO_4$)
32.26	91.6	2.77	Olivine $(Mg_{1.77}Fe_{0.23})SiO_4$)
35.65	70.4	2.52	Olivine $(Mg_{1.77}Fe_{0.23})SiO_4$)
36.46	53.6	2.46	Olivine $(Mg_{1.77}Fe_{0.23})SiO_4$)
38.24	22.0	2.35	Olivine $(Mg_{1.77}Fe_{0.23})SiO_4$)
39.63	33.7	2.27	Olivine $(Mg_{1.77}Fe_{0.23})SiO_4$)
40.00	45.9	2.25	Olivine $(Mg_{1.77}Fe_{0.23})SiO_4$)
41.73	11.3	2.16	Olivine $(Mg_{1.77}Fe_{0.23})SiO_4$)
48.42	9.8	1.88	Olivine $(Mg_{1.77}Fe_{0.23})SiO_4$)
50.91	4.0	1.79	Olivine $(Mg_{1.77}Fe_{0.23})SiO_4$)
52.17	43.4	1.75	Olivine $(Mg_{1.77}Fe_{0.23})SiO_4$)
54.80	11.8	1.68	Olivine $(Mg_{1.77}Fe_{0.23})SiO_4$)
56.07	12.2	1.64	Olivine $(Mg_{1.77}Fe_{0.23})SiO_4$)
56.74	20.1	1.62	Olivine $(Mg_{1.77}Fe_{0.23})SiO_4$)
57.84	5.5	1.59	Olivine $(Mg_{1.77}Fe_{0.23})SiO_4$)
58.66	3.9	1.57	Olivine $(Mg_{1.77}Fe_{0.23})SiO_4$)
61.08	5.8	1.52	Olivine $(Mg_{1.77}Fe_{0.23})SiO_4$)
61.86	73.0	1.50	Olivine $(Mg_{1.77}Fe_{0.23})SiO_4$)
62.63	39.5	1.48	Olivine $(Mg_{1.77}Fe_{0.23})SiO_4$)
66.93	16.7	1.40	Olivine $(Mg_{1.77}Fe_{0.23})SiO_4$)
69.65	14.9	1.35	Olivine $(Mg_{1.77}Fe_{0.23})SiO_4$)
71.60	5.4	1.32	Olivine $(Mg_{1.77}Fe_{0.23})SiO_4$)
85.15	2.3	1.14	Olivine $(Mg_{1.77}Fe_{0.23})SiO_4$)

Peak match citation: PDF 01-075-6789 in Gates-Rector and Blanton (2019)

2.13.2 Chemistry from X-Ray Fluorescence

Table 21. Olivine - Bulk Chemistry

Compound	*Concentration (wt%)*
MgO	44.3
Al_2O_3	0.8
SiO_2	39.6
P_2O_5	1.0
Cl	0.4
CaO	0.4
Cr_2O_3	0.5
MnO	0.2
Fe_2O_3	12.1
NiO	0.7
Total	100.0

2.13.3 FTIR Spectroscopy

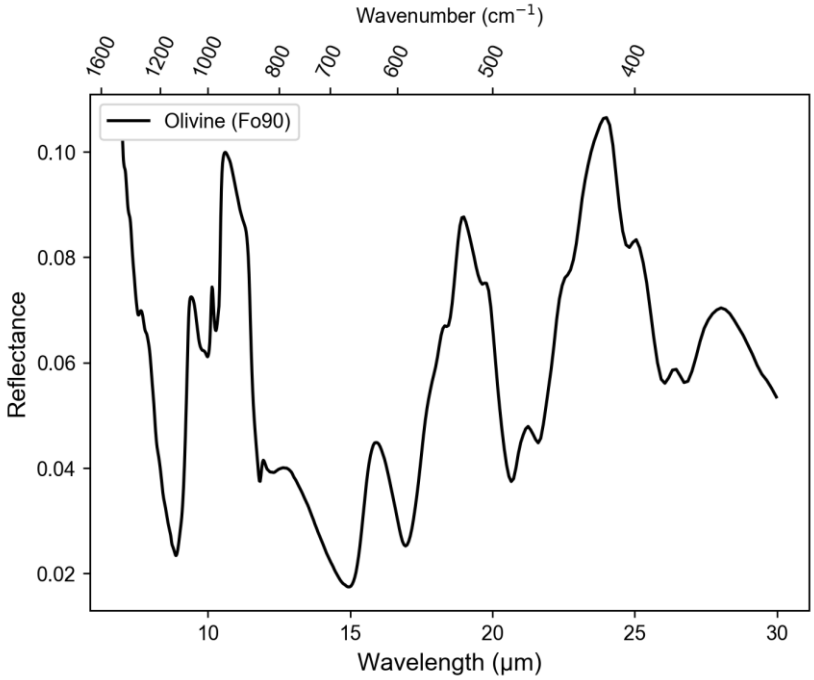

Figure 47. Olivine FTIR Spectroscopy

2.13.4 VIS NIR Spectroscopy

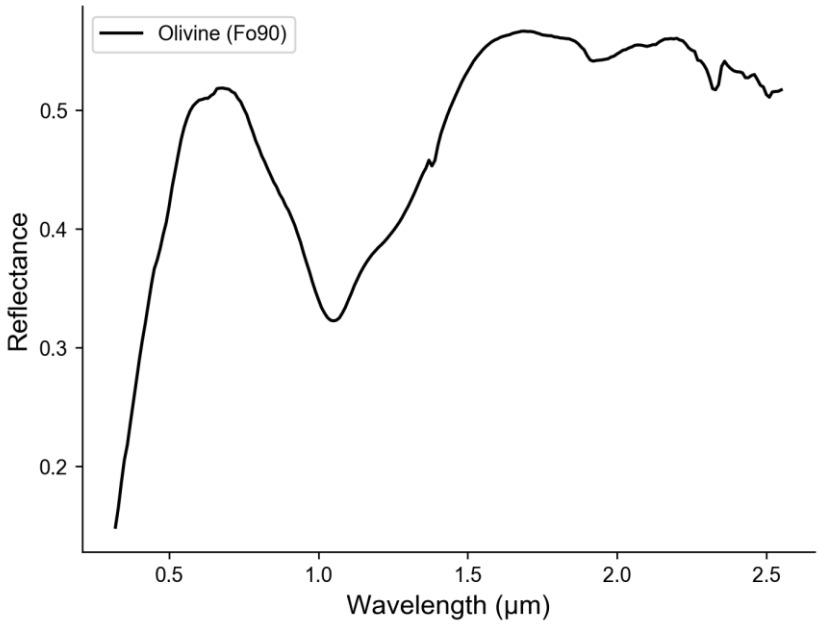

Figure 48. Olivine VIS NIR Spectroscopy

2.13.5 Particle Size Analysis

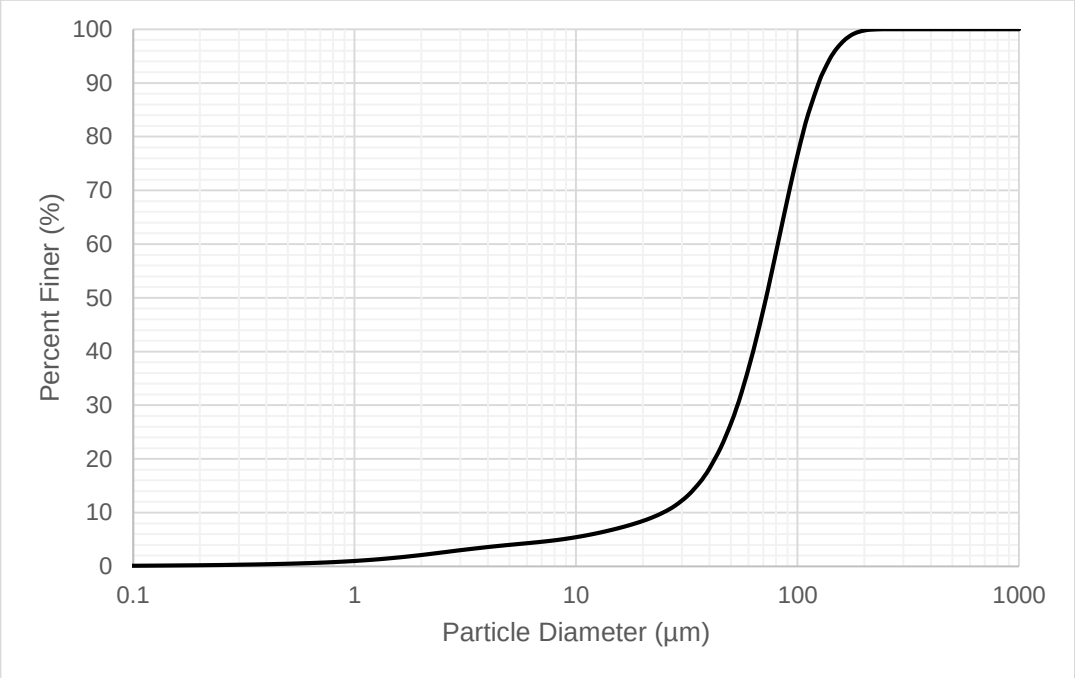

Figure 49. Olivine Particle Size Distribution

2.14 Siderite

• Description: Iron carbonate

• Source: SIDCO Minerals

• Idealized Formula: $FeCO_3$

• Also called: Iron(II) carbonate, ferric carbonate

Notes Major phase confirmed by XRD analysis (Table 22, Figure 51). XRF analysis (Table 23) shows 85% of the mass is made up of iron compounds. Carbon is too light to be detected with our XRF analyzer. There is some evidence of contamination from an aluminum silicate phase in the XRF data, but their relative concentrations would be lower if carbon could be detected and were included in the bulk chemistry quantification.

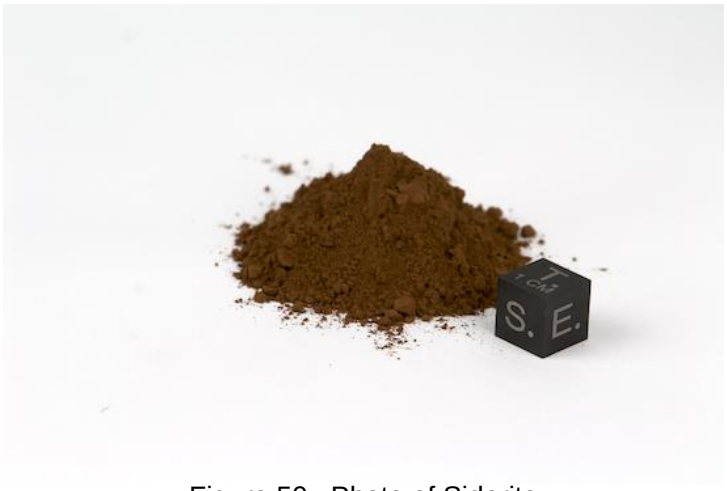

Figure 50. Photo of Siderite

2.14.1 X-Ray Diffraction Pattern

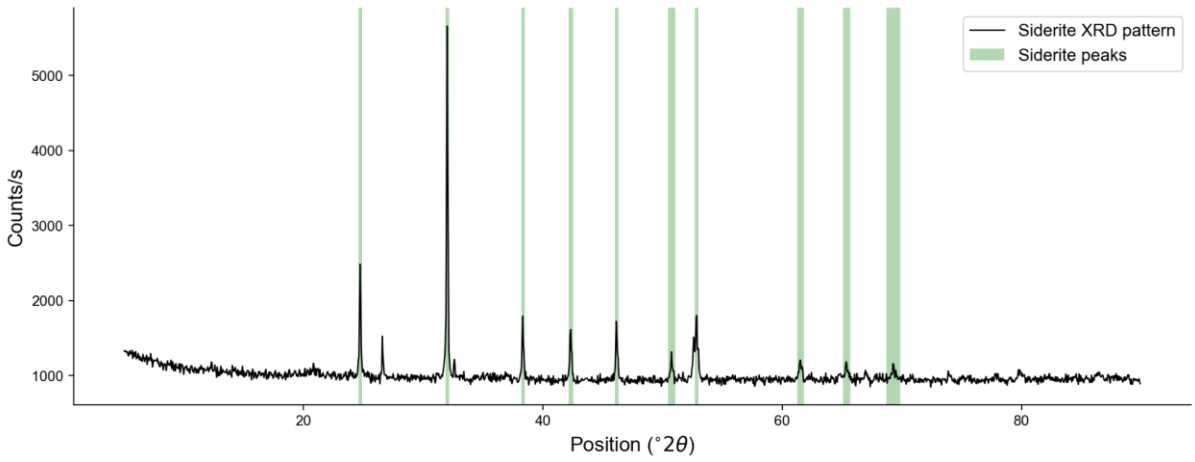

Figure 51. XRD Pattern for Siderite Sample

Table 22. Siderite - XRD Pattern Peaks

Position (°2θ)	*Relative Intensity (%)*	*d-spacing (Å)*	*Matched By*
24.74	37.7	3.60	Siderite
26.62	9.7	3.35	
32.02	100.0	2.80	Siderite
38.33	19.9	2.35	Siderite
42.33	17.6	2.14	Siderite
46.17	16.9	1.97	Siderite
50.76	6.8	1.80	Siderite
52.84	22.0	1.73	Siderite
61.53	6.0	1.51	Siderite
65.40	4.7	1.43	Siderite
69.28	3.4	1.36	Siderite

Peak match citation: PDF 00-029-0696 in Gates-Rector and Blanton (2019)

2.14.2 Chemistry from X-Ray Fluorescence

Table 23. Siderite - Bulk Chemistry

Compound	*Concentration (wt%)*
Al_2O_3	5.0
SiO_2	7.0
P_2O_5	0.9
SO_3	0.4
Cl	0.2
K_2O	0.3
CaO	0.6
TiO_2	0.2
MnO	0.2
Fe_2O_3	85.0
ZnO	0.1
Rb_2O	0.2
Total	99.9

2.14.3 FTIR Spectroscopy

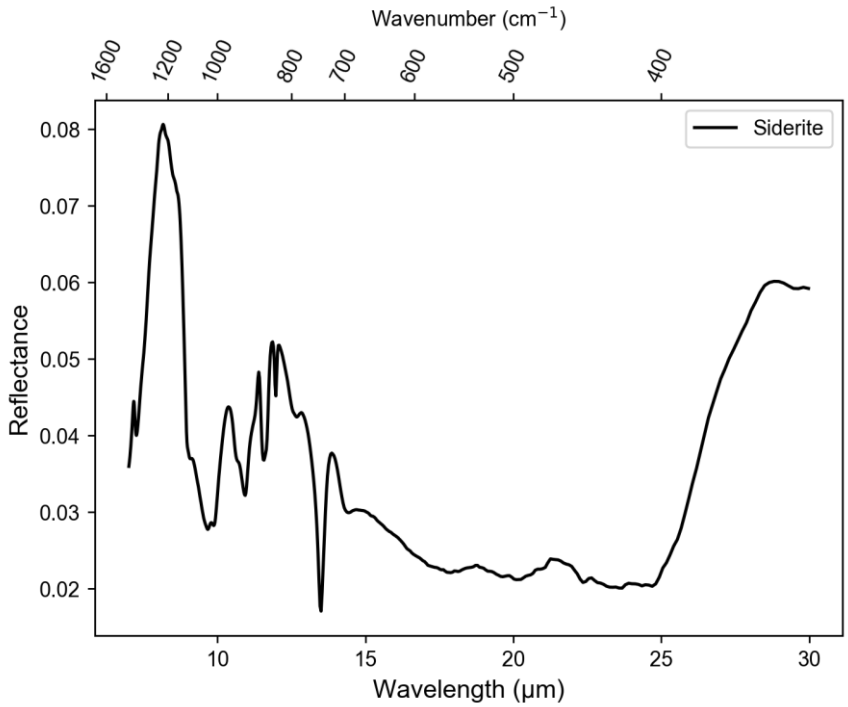

Figure 52. Siderite FTIR Spectroscopy

2.14.4 VIS NIR Spectroscopy

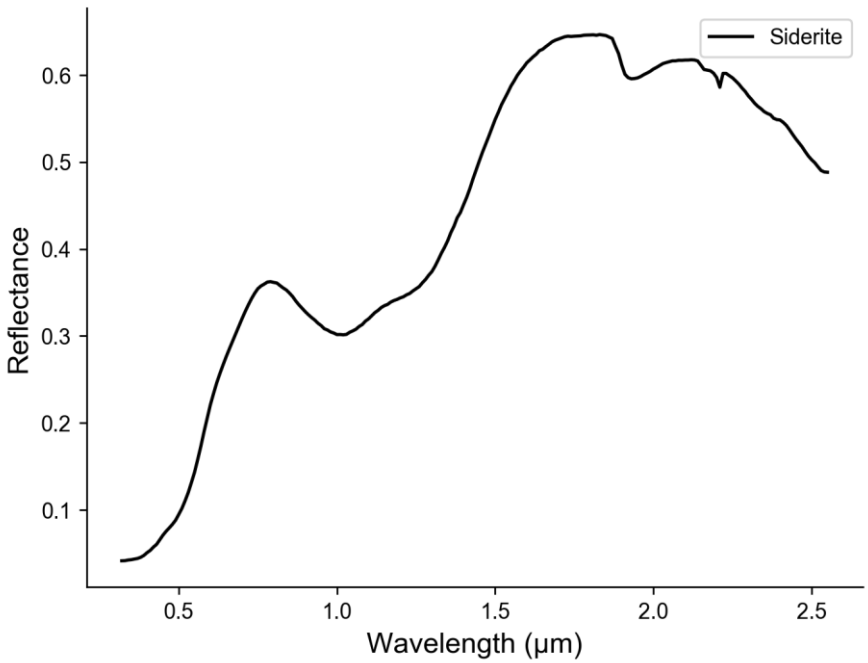

Figure 53. Siderite VIS NIR Spectroscopy

2.14.5 Particle Size Analysis

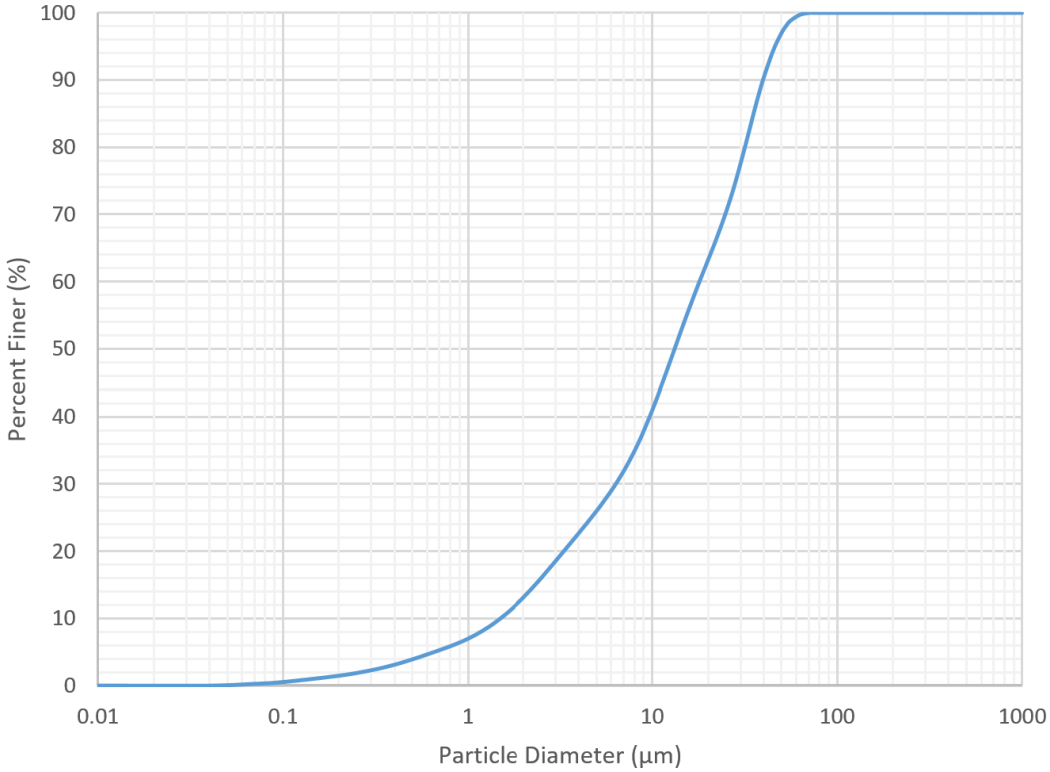

Figure 54. Siderite Particle Size Distribution

2.15 Smectite

• Description: Family of clay minerals

• Source: Aardvark Clay & Supplies (Bentonite, IBEX 200)

• Idealized Formula: $(Na,Ca)_{0.33}(Al,Mg)_2(Si_4O_{10})(OH)2 \cdot nH_2O$ (Montmorillonite, the primary phase in bentonite clay)

Notes XRD analysis confirms the major phases are the smectite-family clays nontronite and montmorillonite (Table 24, Figure 56). Other clays (kaolin and vermiculite) were also detected by XRD, and there were some unidentified XRD peaks. XRF analysis (Table 25) is consistent with primary phases of aluminum, magnesium, calcium, and/or iron silicates.

Figure 55. Photo of Smectite

2.15.1 X-Ray Diffraction Pattern

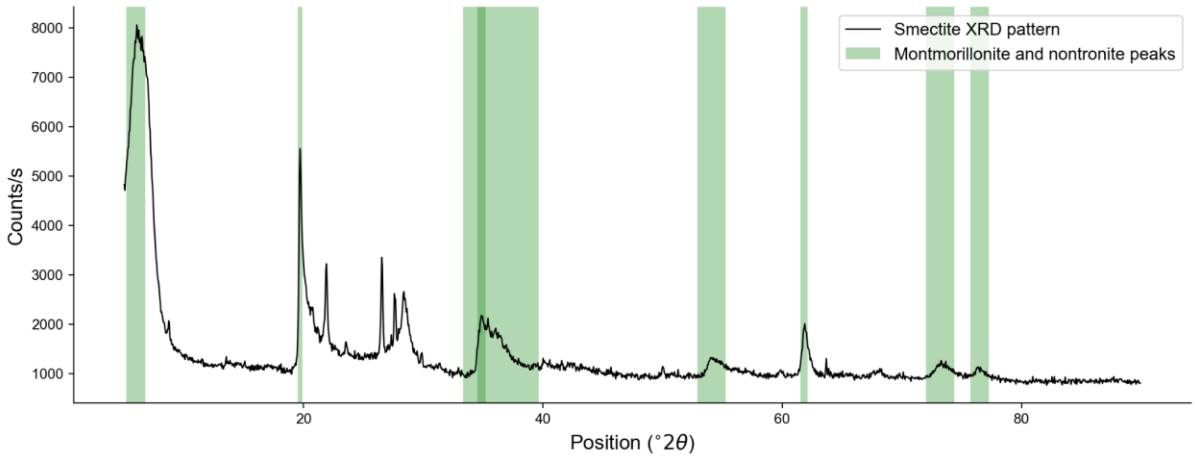

Figure 56. XRD Pattern for Smectite Sample

Table 24. Smectite - XRD Pattern Peaks

Position (°2θ)	*Relative Intensity (%)*	*d-spacing (Å)*	*Matched By*
5.99	100.0	14.76	Montmorillonite, nontronite, vermiculite
7.00	85.6	12.63	Kaolin
19.71	66.3	4.51	Montmorillonite, nontronite, kaolin, vermiculite
21.92	32.6	4.06	
23.56	8.2	3.78	Vermiculite
26.55	34.8	3.36	
27.64	23.0	3.23	
28.37	24.6	3.15	Montmorillonite, vermiculite
34.87	17.8	2.57	Montmorillonite, nontronite, kaolin, vermiculite
36.49	9.4	2.46	Montmorillonite, nontronite, vermiculite
41.98	2.5	2.15	
54.08	5.3	1.70	Montmorillonite, nontronite, kaolin, vermiculite
61.82	15.1	1.50	Montmorillonite, nontronite, kaolin, vermiculite
68.04	2.2	1.38	
73.19	4.9	1.29	Montmorillonite, nontronite, kaolin, vermiculite
76.48	3.8	1.25	Montmorillonite, nontronite, kaolin, vermiculite

Peak match citation: PDF 00-002-0009, PDF 00-002-0017, PDF 00-002-0037, PDF 00-003-0009, and PDF 00-003-0010 in Gates-Rector and Blanton (2019)

2.15.2 Chemistry from X-Ray Fluorescence

Table 25. Smectite - Bulk Chemistry

Compound	*Concentration (wt%)*
MgO	1.8
Al_2O_3	20.3
SiO_2	65.8
P_2O_5	1.1
SO_3	1.1
Cl	0.4
K_2O	0.7
CaO	2.0
TiO_2	0.3
Fe_2O_3	6.5
SrO	0.1
Total	99.9

2.15.3 FTIR Spectroscopy

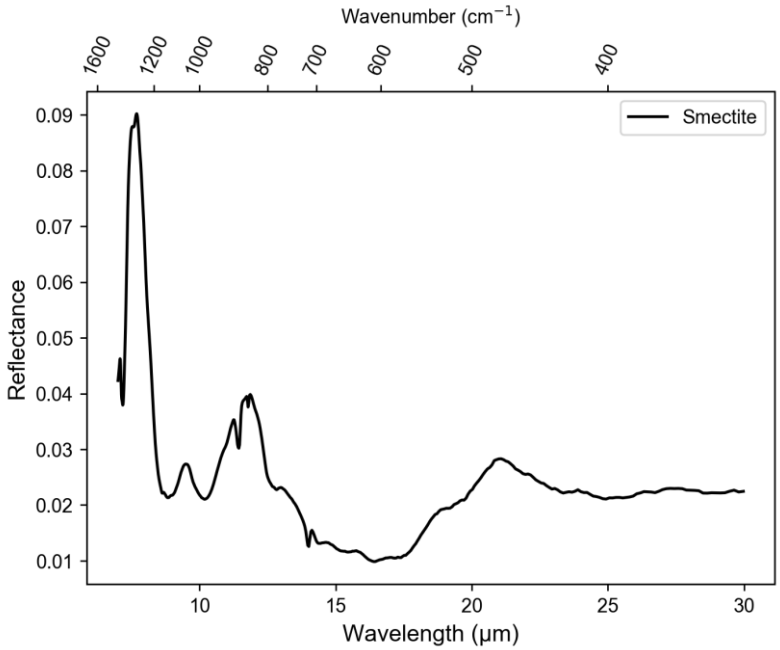

Figure 57. Smectite FTIR Spectroscopy

2.15.4 VIS NIR Spectroscopy

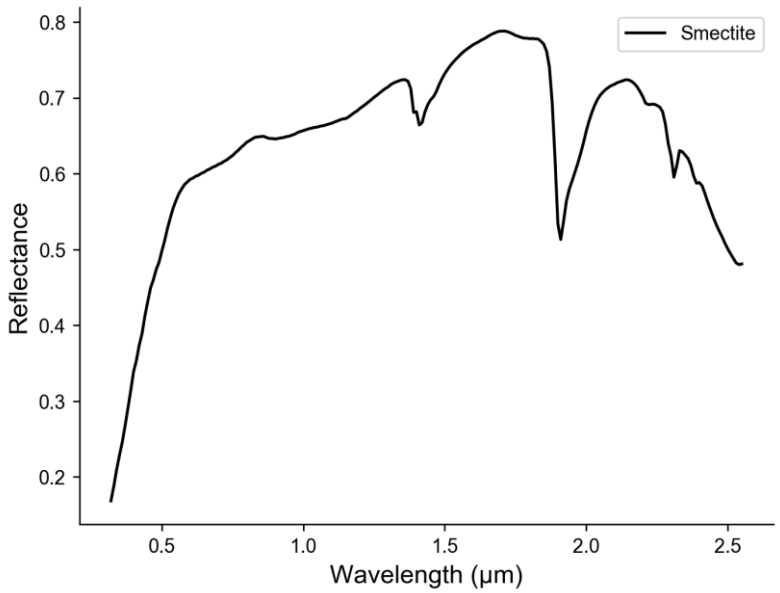

Figure 58. Smectite VIS NIR Spectroscopy

2.15.5 Particle Size Analysis

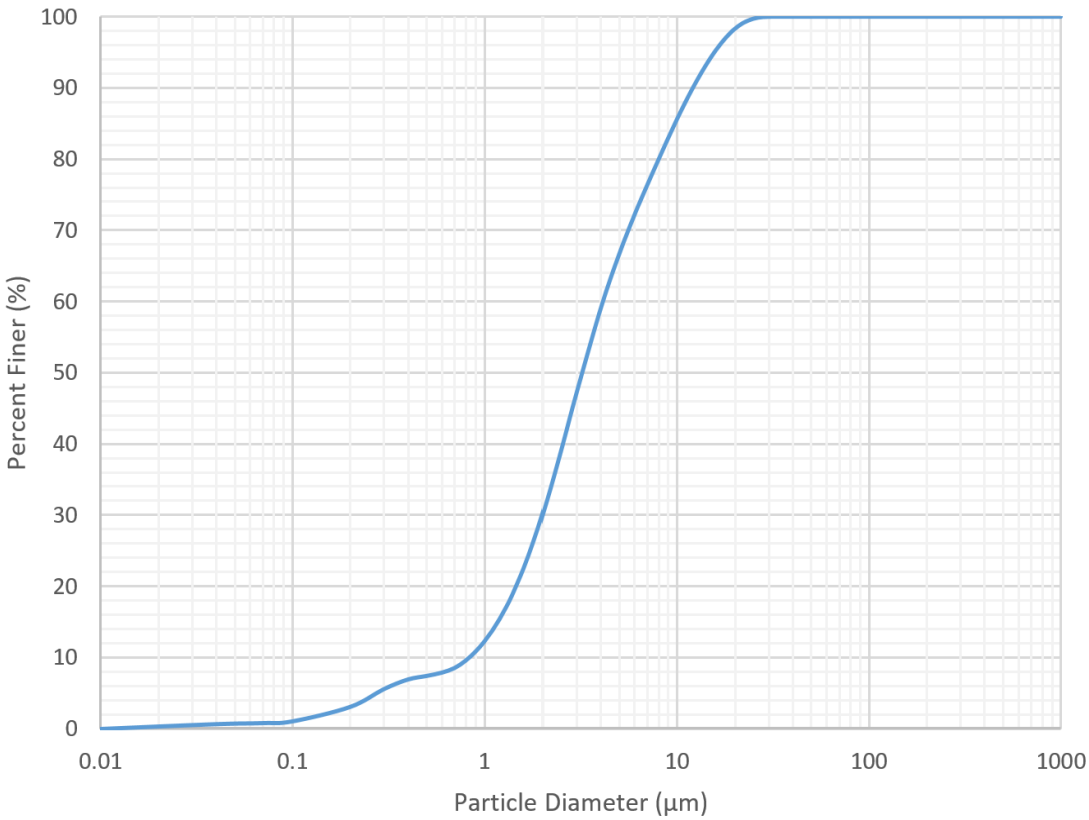

Figure 59. Smectite Particle Size Distribution

3 Acknowledgements

This work was supported by NASA Cooperative Agreement 80NSSC19M0214 to the Center for Lunar and Asteroid Surface Science (CLASS) as part of the Solar System Exploration Research Virtual Institute (SSERVI). This work was also supported by the Florida Space Institute at the University of Central Florida. The Exolith Lab gratefully acknowledges Kirk Scammon for collecting the XRF and XRD data. We also gratefully acknowledge Jesse Colangelo and Luis Zea who provided us with fused disk XRF data for basalt, funded by the University of Colorado, Boulder's Research Innovation Office.

References

Gates-Rector, S. and T. Blanton (2019). The powder diffraction file: a quality materials characterization database. *Powder Diffraction 34*(4), 352–360.

Schofield, P. F., K. S. Knight, and I. C. Stretton (1996, 08). Thermal expansion of gypsum investigated by neutron powder diffraction. *American Mineralogist 81*(7-8), 847–851.

Vaughan, G., R. Brydson, and A. Brown (2012, jul). Characterisation of synthetic two-line ferrihydrite by electron energy loss spectroscopy. *Journal of Physics: Conference Series 371*, 012079.